2014

Microstructure, Quasi-Static, And High-Strain Rate Dynamic Characterization Of Metakaolin And Fly Ash Based Geopolymers For Structural Applications

Damian Lee Stoddard
University of Mississippi

MICROSTRUCTURE, QUASI-STATIC, AND HIGH-STRAIN RATE DYNAMIC CHARACTERIZATION OF METAKAOLIN AND FLY ASH BASED GEOPOLYMERS FOR STRUCTURAL APPLICATIONS

A Thesis
Presented in Partial Fulfillment of Requirements
for the Degree of Master of Science
in the Department of Mechanical Engineering
The University of Mississippi

by

DAMIAN L. STODDARD

November 2013

ABSTRACT

Geopolymers are a class of rapid setting cementing systems that have been used as mortar or additives in concrete mixes to improve properties. Several types of geopolymer systems such as metakaolin and fly ash based geopolymers are widely used, and are available in different mixture proportions [1, 2]. Metakaolin ($Al_2Si_2O_7$), a dehydroxylated form of Kaolinite ($Al_2Si2O5(OH)_4$) clay readily available from many sources, provides several benefits when added to a concrete mix design or used as a mortar system, including durability, freeze/thaw, acid resistance, and high temperature resistance [3]. Class F fly ash-based mortar geopolymers provide added fire retardation, reduces crack formation, etc., when added to a concrete mix or used as a mortar system. This thesis compares the quasi-static and dynamic properties of both a pure metakaolin geopolymer and a fly ash based geopolymer material system that utilizes siliceous sand as fine aggregate. Microstructural characterization studies included Scanning Electron Microscope (SEM), Energy Dispersive Spectroscopy (EDS), X-Ray Diffraction (XRD), X-Ray Fluorescence (XRF), and Thermal Gravimetric Analysis (TGA). The mechanical properties were evaluated from nanoindentation and monotonic experiments. Spatially correlated nanoindentation and EDS provided mechanical property information (modulus and hardness) and elemental data of individual phases in the samples.

Metakaolin and fly ash based geopolymers are two fundamental alternative cementitious binder materials that can be used to produce sustainable mortars and concretes. While there is limited information related to the quasi-static properties of these materials, no information exists related to their high strain rate mechanical behavior. A Split-Hopkinson Pressure Bar (SHPB)

was utilized to determine the high-strain rate compressive properties of both pure Metakaolin and Class F fly ash geopolymers with sand as fine aggregate. SHPB compressive data for Metakaolin and Class F Fly ash-based mortar along with a Portland Cement-based mortar for comparison are presented. Punch-shear response of the candidate material systems under low-velocity impact is also presented.

DEDICATION

This thesis is dedicated to my mother, father, siblings, and fiancé who motivated me to achieve great things in life and always supported my goals and helped me through obstacles.

LIST OF ABBREVIATIONS AND SYMBOLS

SEM – Scanning Electron Microscope

EDS – Energy Dispersive Spectroscopy

XRD – X-Ray Diffraction

TGA – Thermo Gravimetric Analysis

SHPB – Split Hopkinson Pressure Bar

LOEG – Laser Occlusion Expansion Gage

ACKNOWLEDGMENTS

I would like to first thank Dr. P. Raju Mantena, Professor of Mechanical Engineering for his constant support and assistance through my research and Master's Thesis. Through his guidance my thesis and also knowledge in the field of mechanical engineering has increased tremendously.

I would also like to thank my Graduation Committee, Dr. A. M. Rajendran, Professor and Chair of Mechanical Engineering, and Dr. Tyrus McCarty Associate Professor of Mechanical Engineering for their guidance in preparing my thesis.

I would also like to thank the staff and faculty members in the Department of Mechanical Engineering for their contributions during my graduate study at The University of Mississippi. I would like to thank my colleagues, Dr. Tezeswi Tadepalli, Brahmananda Pramanik, Kiyun Kim, and Andy Gossett for their assistances in many aspects of my research.

I would also like to thank several key individuals at The Engineer Research and Development Center in Vicksburg, Mississippi. I would like to first thank Dr. Robert Moser, Dr. Paul Allison, Dr. P. G. Malone and Mr. Wayne Hodo for helping increase my knowledge of microstructural characterizations techniques and cementitious materials. I would like to thank Mr. Bret Williams, Mrs. E Rae Gore, and Mr. Jedadiah F. Burroughs for their assistance in testing and help with equipment use.

This research was supported by US Army Research Office under the DOD-PIRT sub-contract through North Carolina A & T University Grant No. 300223243A.

I would lastly like to thank my mother, father, siblings, and fiancé for the immense support through my progress of my Master of Science in Mechanical Engineering.

TABLE OF CONTENTS

Page

Page

Page

LIST OF TABLES

Table **Page**

LIST OF FIGURES

Figures **Page**

Figures **Page**

Figures **Page**

Figures **Page**

CHAPTER I. INTRODUCTION AND BACKGROUND

Many materials have been developed over the years to ensure protection against blast, ballistic and impact. These structures must withstand high stresses, ballistic penetration, and large and sudden increases in pressure to ensure survival of the structure and occupants. During blast, ballistic, and impact scenarios structures are required to absorb large amounts of energy due to foreign object penetration, shock, local punch shear, and thermal stresses. Generally large structures exposed to blast, ballistic, and impact scenarios are made of concrete. Concrete has very high compressive properties in comparison to many materials, however cementitious alternatives such as geopolymers are slowly emerging and replacing structural applications that ordinarily would use concrete.

This research is focused on comparing the microstructure of a Metakaolin geopolymer and a fly ash-based mortar geopolymer with a conventional Portland cement-based mortar. Only one mix design for each material is compared using several techniques for microstructural, quasi-static, and dynamic characterization.

I.I Geopolymers

Many additives and cementitious substitutes have been used in concrete over the years one of them being geopolymers. Geopolymers have been used in concrete mixes to cut cost, increase strength, improve chemical resistance, reduce permeability, reduce the amount of waste material, and enhance the workability. Geopolymers are a class of rapid setting cementitious alternatives used for high temperature ceramics, fire and heat resistant coatings and adhesives,

binder for fire resistant composites, and toxic and radioactive waste encapsulation. Another application that geopolymers have been considered for are adhesives between metals or metals and glasses. Geopolymer depend on the interaction of strong alkali solutions with a variety of finely particulate disordered alumino-silicates; predominantly glassy materials (e.g. slag, fly ash) or clays fired to reduce their crystallinity (metakaolin). Generally, these products are made by reacting a mixture of sodium or potassium hydroxide and sodium silicate with a glass or near amorphous solid that is rich in aluminum and silica. This interaction of strong alkali and disordered alumino-silcates produces an alumino-silcate gel that consists of silicate and aluminates tetrahedrally bonded in complex networks with oxygen bridges [4, 5]. Figure 1.1 shows typical structures for silicate and aluminates tetrahedrally bonded in complex networks with oxygen bridges.

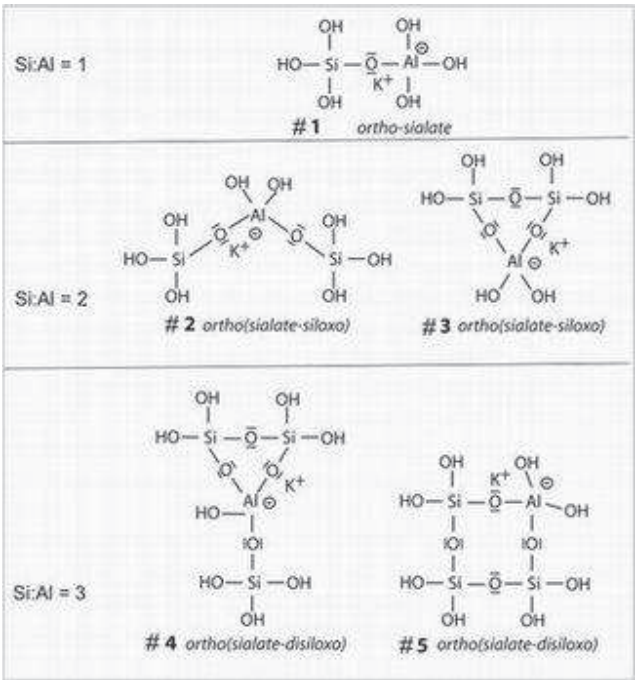

Figure 1.1 Silicate and Aluminate Tetrahedrally bonded in Complex Networks with Oxygen Bridges [6]

The reactants can be fine-grained products such as coal-derived fly ash, ground granulated metallurgical slags, or even combusted waste material such as rice hull ash. The reaction can take place at normal laboratory temperature or elevated temperatures (typically in the range of 30 °C to 50 ˚C). Moist curing is typically used to assure a rapid strength gain. The reactants form a series of alumino-silicate chains or networks of oxygen, silicon aluminum linked with covalent bonds. Geopolymers are differentiated from other cements in that the hardened material is practically an X-ray amorphous solid at ambient and medium temperatures, and only becomes crystalline at temperatures above 500 ˚C. The most commonly used geopolymers are complex alumino-silicate gels that consist of silicate and aluminate tetrahedrally bonded in complex networks with oxygen bridges [6].

A wide variety of research has been conducted on metakaolin and fly ash including the microstructural, chemical resistance, strength at varying cure times and mix proportions. However, there is very limited information on the high-strain rate and low-velocity impact response of these candidate material systems that are being considered for blast and impact mitigation applications. In this thesis, the high-strain rate compressive properties and the punch-shear response of both metakaolin and the fly ash based geopolymer material systems are presented.

Despite the vast array of information related to material mixture proportioning, and quasi-static mechanical properties, high strain rate and low-velocity impact data has not been reported in open literature. Due to the growing threat of structures being subjected to impact situations a detailed investigation of any material, including geopolymers, used in structural applications is merited.

I.I.I Metakaolin

As previously stated Metakaolin is a dehydroxylated form of Kaolinite ($Al_2Si_2O_5(OH)_4$) clay. Figure 1.2 shows a typical unreacted sample of metakaolin.

Figure 1.2 Unreacted Sample of Metakaolin [7]

Initially disordered or ordered Kaolinite clay is heated at temperature of 530 ˚C to 630 ˚C causing dehydroxylation. Figure 1.3 shows the dehydroxylation process for a typical alumino-silicate.

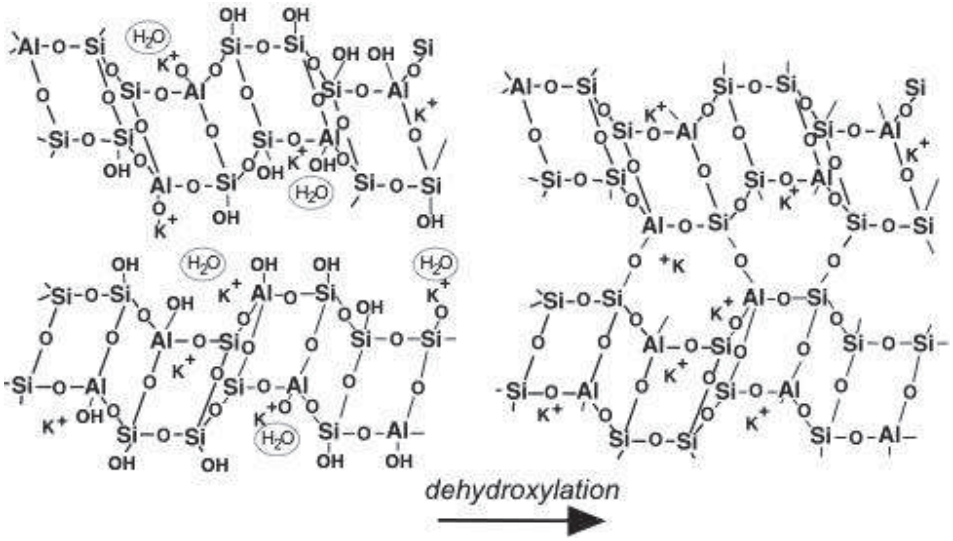

Figure 1.3 Dehydroxylation of Alumino-Silicate Compound [6]

Above the dehydroxylation temperature kaolinite is converted to a complex ordered amorphous metakaolin. Once kaolinite has been converted into metakaolin the octahedral layer converts to

tetrahedrally and pentahedrally coordinated. Metakaolin is a complex amorphous structure that retains some long range order due to layer stacking. It is crucial to heat kaolinite to a point of complete dehydroxylation to produce highly reactive pozzolan. A pozzolan is a siliceous or aluminous and siliceous material which is not a cement by itself, but when combined with a hydroxide compound such as sodium hydroxide forms a compound that has cementitious like properties. Once this complete dehydroxylation is done an amorphous, highly reactive pozzolan compound is formed.

Metakaolin has many advantages and uses in concrete design. Some advantages when using metakaolin in a concrete mix design are increased durability, reduced effects of alkali-silica reactivity, reduced shrinkage due to particle packing making the concrete denser, enhanced workability and finish of concrete, increase resistance to chemical corrosion, reduced permeability, increase flexural and compressive strength, and reduced potential of efflorescence. Typical uses of metakaolin in concrete design are high performance, high strength, and light weight concretes, mortars, glass fiber reinforced concretes, fibercement and ferrocement products, precast and pour molded concrete, and an adhesive.

I.I.II Class F Fly Ash-Based Mortar

Fly ash is a residue that is produced from combustion. During the combustion process the combustion residue floats and is captured before leaving the chimney of most industrial plants. The fly ash residue that is produced from the combustion has a chemical composition of amorphous and crystalline silicon dioxide (SiO_2) and calcium oxide. A typical sample of fly ash is shown in Figure 1.4.

Figure 1.4 Typical Fly Ash Sample [8]

Because of the nature of production of fly ash toxic chemicals such as arsenic, boron, cadmium, cobalt, chromium, mercury, lead, manganese, molybdenum, selenium, strontium, vanadium, and thallium may be present in the fly ash residue. Approximately 43% of fly ash that is produced in the U.S. is recycled and used in Portland cement concretes and mortars. Because fly ash contains toxic contaminates health concerns have been raised, but to alleviate any issues the bottom ash that does not fly to the top of the chimney, which usually contains less contaminates than the top fly ash, and the top fly ash are mixed to bring the contaminate levels within nonhazardous waste guidelines.

While suspended inside exhaust gases fly ash solidifies rapidly and is collected. Because of the rapid solidification the shape of the fly ash particles are spherical. The particle size ranges from 0.5 μm to 300 μm. Since the cooling process is rapid amorphous, quenched glass remains and a small fraction of crystallized particles are present. As a result of this process fly ash is heterogeneous and contains SiO_2, Al_2O_3, Fe_2O_3 and occasionally CaO. ASTM C618 [9] is used as a guideline to define two types of fly ash, class C fly ash and class F fly ash. The difference between the two fly ashes is the amount of calcium, alumina, silica, and iron present in the fly

ash. Based on the material that is combusted, the composition of the fly ash material changes. Different applications require different compositions of fly ash. Fly ash that is used as an additive in a concrete or mortar mix design or as a cement replacement in structural applications must meet strict construction standards. To meet structural guidelines 75% of the fly ash must have a fineness of 45 μm or less and have a carbon content of less the 6%. Fly ash can also be used to form a geopolymer that has comparable properties as hydrated Portland cement and having less CO_2 emissions.

Class C fly ash is produced from the combustion of subbituminous coals and less aged lignite. This particular class of fly ash has pozzolanic properties, and has self cementing properties with the addition of water. Because of this self cementing property in the presence of water, class F fly ash will harden and gain strength over time. This self cementing process does not need an activator. Alkali and sulfate content is higher in class C fly ash when compared to class F fly ash.

Class F fly ash is produce from the combustion of bituminous coal and more aged anthracite. Class F fly ash contain less than 20% lime (CaO) and is pozzolanic. The glassy silica and alumina in class F fly ash need an activator to produce a cementitious compound because of the pozzolanic nature of the material. Activators that can be used to intiate the cementing process are Portland cement, quicklime, or hydrate lime in the presence of water or a solution of sodium silicate. Using sodium silicate as an activator forms a geopolymer. [10]

I.II Microstructural Characterization

Many methods for microstructural characterization of materials have been used over the years. Several methods typically used when researching new materials are Scanning Electron

Microscope (SEM), Energy Dispersive Spectroscopy (EDS), X-Ray Diffraction (XRD), and Thermo Gravimetric Analysis (TGA). These methods provide information about micro cracks, elemental composition, crystalline structures, and phases in the material observed.

I.II.I Scanning Electron Microscope (SEM)

SEM is a type of microscope that uses a focused electron beam to produce highly magnified images with resolution exceeding 1 nanometer. The focused electron beam is scanned in a raster scan pattern and the signal of the beam is detected by a detector to produce an image. SEM can be used in high vacuum and low vacuum mode depending on the magnifications required. Usually secondary electrons are detected and the quantity is dependent on the angle made between the surface and the beam. Images of the tilt of the surface are then displayed. There are several types of signals a SEM produces one such is back scattered electrons. Back scattered electrons reflect from the sample and the signal is strongly related to the atomic number of the specimens, which allows for the elements in the sample to be identified. Due to the large depth of field caused by the extremely narrow electron beam three dimensional images can be achieved. Samples for SEM must fit inside the confines of the SEM and be securely mounted on the specimen stage. The SEM use for analysis is shown in Figure 1.5.

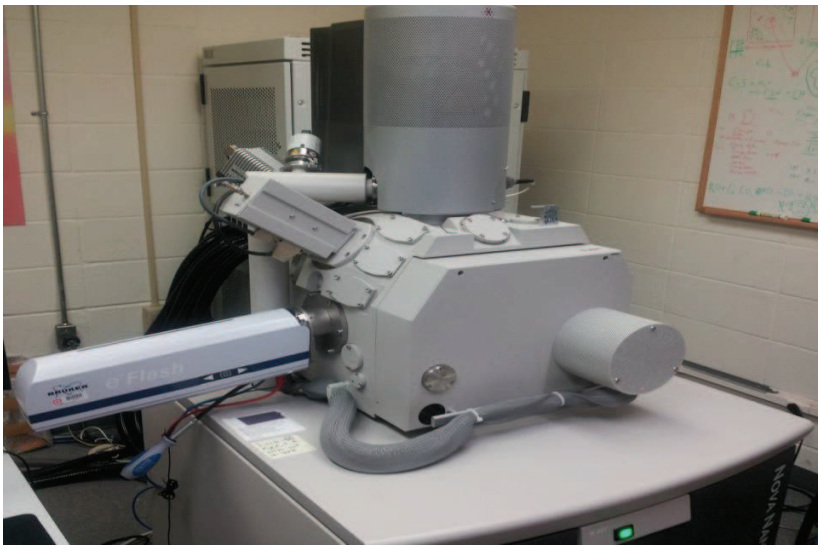

Figure 1.5 FEI Nova NanoSEM 630 field emission variable-pressure Scanning Electron Microscope Used for Microstructural Analysis [11]

Many SEMS have the ability to rotate the specimen stage, and also tilt the specimen stage. Specimens are generally electrically conductive at the surface and are electrically ground to prevent electrostatic charges from accumulating at the surface of the specimen. Samples that are not electrically conductive usually charge from the electron beam causing artifacts on the image in high vacuum mode, so images are usually viewed in low vacuum mode. To prevent the appearance of artifacts in high vacuum mode, nonconductive samples are coated with highly conductive materials such as gold, platinum, tungsten, etc. by a process known as sputter coating. Sputter coating deposits a thin layer of material by either low vacuum sputter coating or high vacuum evaporation. Specimens are usually mounted in an epoxy and cut to expose the surface of the sample. Specimens prepared for SEM must by ground to an ultra smooth polish so that quantitative X-ray information can be obtained. [12]

The FEI Nova NanoSEM 630 field emission variable-pressure SEM was used to observe different phases in materials, micro crack paths, impurity content and void content in samples.

Comparing the phases could show why certain materials have higher strength properties than other materials based on the phases that are present in the material. The the micro crack paths can also be followed using the FEI Nova NanoSEM 630 field emission variable-pressure SEM.

I.II.II Energy Dispersive Spectroscopy (EDS)

EDS can be done in unison with SEM. EDS is an elemental analysis technique used to characterize the elemental composition of a sample. Figure 1.6 shows the EDS analysis attachment that is attached directly to the SEM.

Figure 1.6 Bruker Quantax AXS Solid-State EDX Detector Energy Dispersive Spectroscopy Analysis Attachment [13]

EDS depends on the unique signals for specific structures due to an X-ray excitation. To excite the characteristic X-rays for specimens a high energy beam of electrons, protons, or X-ray is used. The beam excites an electron in an inner shell causing it to be expelled from its location. This creates a vacancy where the electron was which is then filled by an electron from a higher

outer shell. The energy difference between the higher energy shell and the lower energy shell is released as X-ray. The X-ray emitted from a specimen can be measured by an energy dispersive spectrometer. Since the atomic structure of elements are different, the X-ray signal emitted is easily used to measure the specific type of element that emitted the signal. Samples with overlapping peaks can be a source of error when conducting EDS. EDS specimens must be prepared using the same procedure as SEM samples. [14, 15]

EDS analysis was used to gather chemical composition data for the materials compared. Using the elemental composition data, comparison between theoretical data and EDS signal can be done. This comparison will ultimately validate if the mortars and geopolymer elemental composition is consistent with chemicals that were used in the batching process, and will also give elemental information about impurities present in the mortars and geopolymers.

I.II.III X-Ray Diffraction (XRD)

XRD is a method for identifying crystalline structure materials. During XRD randomly oriented crystals are bombarded with X-rays and gradually rotated. This bombardment of X-rays produces a diffraction pattern consisting of reflections. The X'Pert Pro Diffractometer XRD analysis equipment used in this report is shown in Figure 1.7.

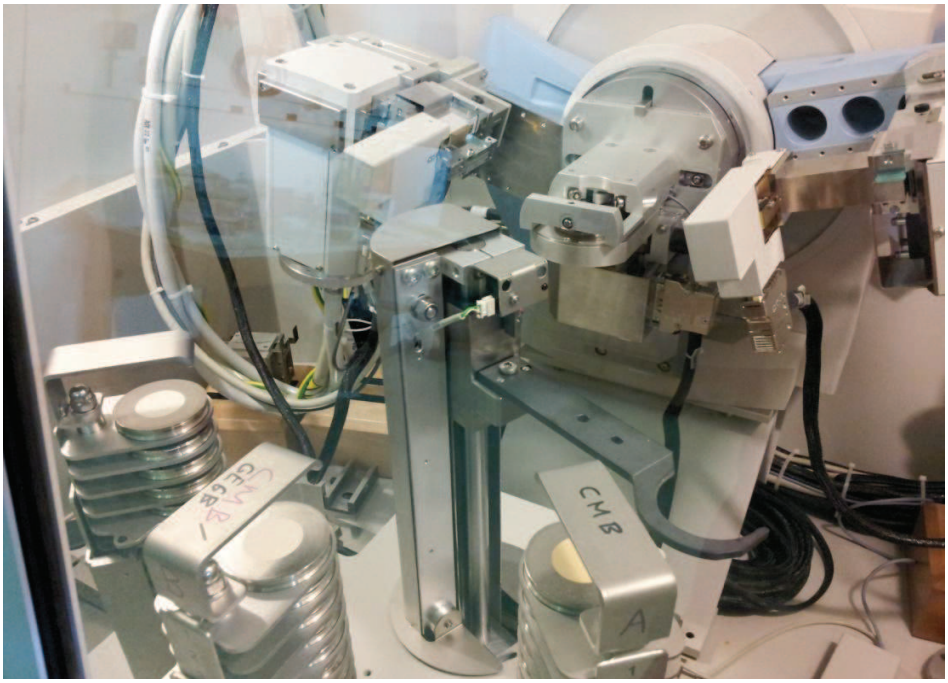

Figure 1.7 X'Pert Pro Diffractometer X-Ray Diffraction Analysis Apparatus [16]

These reflections are regularly spaced based on the type of crystal structure. Based on the amplitude of reflections, crystalline makeup of the sample can be obtained. [17]

The XRD setup was used in this analysis to compare the crystalline makeup of the mortars and geopolymers for comparison with theoretical crystalline makeup and to acquire data about impurities. The XRD was also used to see if there is any correlation between the crystalline makeup and monotonic and dynamic strength.

I.II.IV Thermo Gravimetric Analysis (TGA)

Thermo Gravimetric Analysis measures changes in chemical and physical properties as a function of increasing temperature. TGA analysis can provide information about adsorption, absorption, vaporization, sublimation, desorption, and second order phase transition. TGA can also provide information about dehydration, chemisorptions, oxidation, reduction, and

decomposition. The STA 449 F1 Jupiter Thermo Gravimetric Analysis Machine used for analysis is shown in figure 1.8.

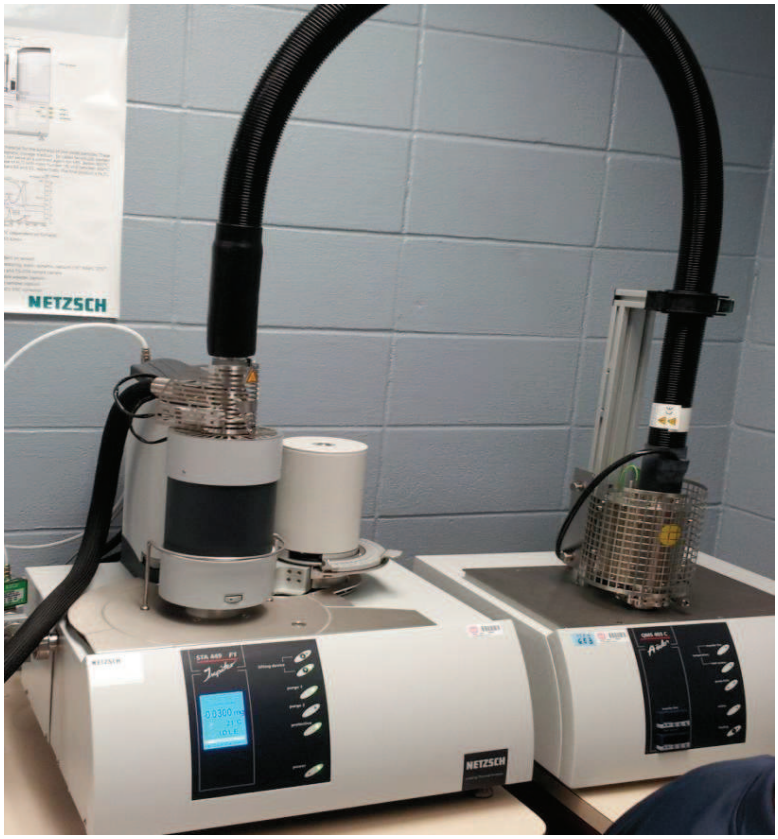

Figure 1.8 STA 449 F1 Jupiter Thermo Gravimetric Analysis Machine [18]

Materials that exhibit mass loss or gain due to decomposition, oxidation, or loss of volatiles such as water are usually studied using TGA. The main applications for TGA are material characterization by decomposition, determination of organic compounds, determination of inorganic compounds, and degradation. A TGA system relies on three precisely measured values for temperature, temperature change, and mass change. TGA systems require a precision balance and a sample placed inside a pan. The furnace system of the TGA system must be programmable so that a constant heating rate can be applied to the sample. TGA furnace systems can also apply a constant mass loss rate. While a constant mass loss type of analysis is

less common then a constant heating rate, it can provide information about reaction kinetics. TGA samples are prepared by grinding samples into a fine powder. [19]

Using the TGA setup crucial data about the phases present in the mortars and geopolymers can be obtained. Because specific phases present in each material degrade at different temperatures, information about mass loss or gain can be used to deduce the phases present in the material and also the amount of material present. Using this information the phases of each material can be constructed.

I.III Monotonic Testing

Monotonic loading is a type of testing in which load is applied to a sample at very slow rates of loading so that equilibrium in the sample is achieved. Monotonic loading can give information such as ultimate compressive strength, ultimate tensile strength, hardness, Poisson's ratio, strain to ultimate failure, and stress versus strain graphs.

I.III.I Nanoindentation

Nanoindentation testing can provide engineers with mechanical properties such as Modulus of Elasticity and hardness. The U9820A Agilent Nano Indenter G200 used in this analysis is shown in Figure 1.9.

Figure 1.9 U9820A Agilent Nano Indenter G200 Used for Monotonic Analysis [20]

Nanoindentation can be performed with several types of tips such as three sided pyramidal, cono-spherical, flat-ended, cube corner, Berkovich, sharp conical, blunt conical, Vickers, and flat punch. Figures 1.10-1.12 show some typical tips that are used during nanoindentation.

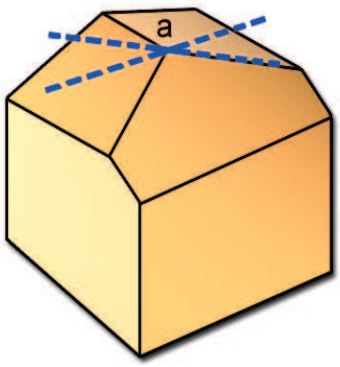

Figure 1.10 Cube Corner and Berkovich Nanoindentation Tip [21]

The cube corner and berkovich tip geometry differs only in the angle of the corner. The cube corner has an angle of 90 ˚ and the Berkovich tip has an angle of 142.35 ˚.

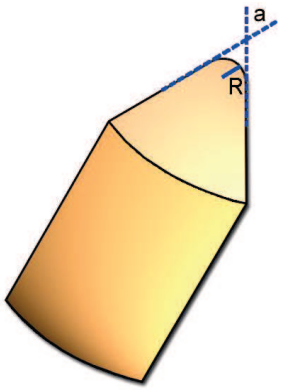

Figure 1.11 Cono-Spherical Nanoindentation Tip [21]

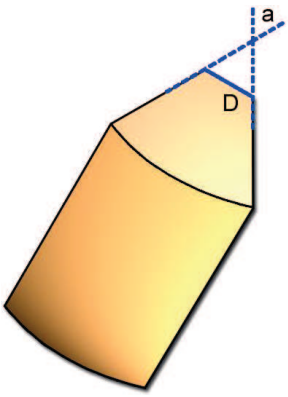

Figure 1.12 Truncated Conical and Cylindrical Punch Nanoindentation Tips [21]

Each configuration of tips can provide more accurate results depending on what type of material is being indented. Tips for nanoindenters are made of extremely hard materials such as diamond, and the mechanical properties of the material are well known. Tip size usually varies from 200 μm to 400 μm. The tip is loaded onto the sample of unknown properties. The tip is loaded into the sample until a specified load is achieved. After the specified value of load has been achieved the load can be held for a set amount of time or released. Load and depth of penetration is used to produce load versus displacement curves. Using the load versus displacement curve mechanical properties can be extracted. Calculations of modulus of elasticity are limited to, linear, isotropic materials. Samples used for Nanoindentation are prepared in the same polishing procedure as the samples prepared in SEM analysis. [22]

For the nanoindentation analysis a Berkovich tip was used to collect hardness and elastic modulus of the materials. The advantage of using the nanoindenters as opposed to conventional monotonic loading condition is the nanoindenter will allow information about the elastic modulus, and hardness profile in a heterogenous sample. This profile is obtainable because the size of the indenter tip is smaller than most of the heterogeneous components of the mortar and geopolymers.

I.III.II Quasi-Static (Compression and Tension)

Quasi-static loading for compression and tension is a process of loading a sample as close to static condition as possible. Tests are usually performed using an Instron, or MTS machine. Figure 1.13 and 1.14 shows an Instron testing machine and a MTS machine respectively.

Figure 1.13 Instron 5980 Floor Model Universal Testing Systems Machine [23]

Figure 1.14 EnduraTec Testing Machine [24]

Loading rates of 0.01/s are used to load the sample so that load equilibrium throughout the sample is met. Mechanical properties such as modulus of elasticity, shear modulus, Poisson's ratio, stress, strain, and ultimate strength can be obtained using this method of material testing. Loading can be performed using load control in which a specified rate of loading is achieved or displacement control in which a specified rate of displacement is achieved. Samples are prepared in different geometric configuration depending on desired mechanical properties such as cylinders for compression test and dog bone, or Brazilian disc specimens for tension test.

For the quasi-static compression and tension cylindrical samples having an aspect ratio of one were used. The diameter of the samples was 16 mm. This small compact size allowed a direct comparison between the results obtained from monotonic loading and Split Hopkinson Pressure Bar. The data that can be obtained from this type of experimental setup is compressive and tensile elastic modulus, strain to ultimate failure, and stress versus strain graphs.

I.IV Dynamic Testing

Dynamic testing is used to characterize materials under dynamic loading conditions. Based on the rate of loading materials can exhibit vastly different properties when compared to quasi-static loading rates. This type of loading can cause large increases in ultimate strength, decrease in strain to failure, increase in energy absorption, increase or decrease in ductility, and changes in other material responses.

I.IV.I Low-Velocity Impact

The low-velocity impact testing is used to test materials at lower strain rates compared to Split Hopkinson Pressure Bar. This information is crucial in determining the penetration strength of a material in a low-velocity impact scenario such as a low speed vehicle impact. Figure 1.15 shows a Dynatup low-velocity impact testing machine.

Figure 1.15 Dynatup 850 Low-Velocity Impact Testing Machine [25]

Typical velocities for this type of setup range from 1 m/s to 10 m/s. The machine can be setup to do several types of loading configurations such as punch shear and Charpy testing.

The information that is obtained from this testing setup is energy absorption for two different phases in loading, and ultimate penetration or punch-shear strength. This can then be compared to other mechanical properties from quasi-static loading condition.

I.IV.II Split Hopkinson Pressure Bar (SHPB)

Split Hopkinson Pressure Bar is used to dynamically load samples in tension, compression, torsion, and punch shear. The compressive SHPB used for this research is shown in Figures 1.16 and 1.17.

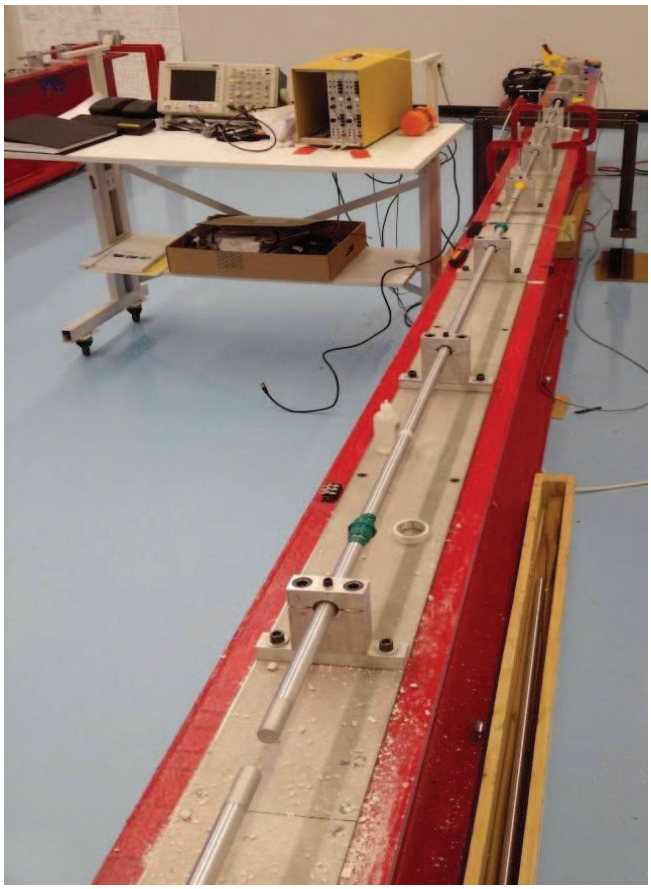

Figure 1.16 Split Hopkinson Pressure Bar at the University of Mississippi Blast and Impact Dynamics Laboratory

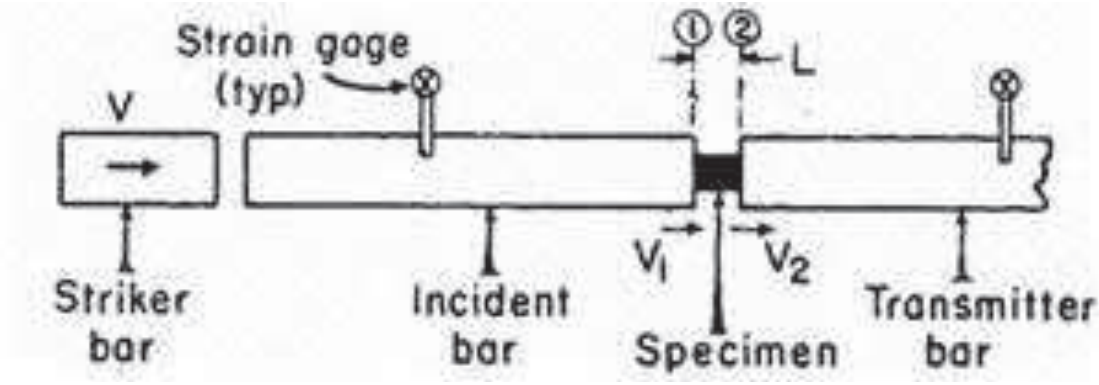

Figure 1.17 Schematic of Split Hopkinson Pressure Bar Setup [26]

Stress and strain relationships for materials under dynamic loading can be obtained using this SHPB system. Typically a striker bar is launched using pneumatic or spring loaded towards an incident bar of significantly longer length than the striker bar. Upon contact of the striker bar and incident bar, a uniaxial stress wave known as the incident wave is generated through the incident bar proportional to the length of the impacting striker bar. The generated stress wave continues until the specimen is reached. Once the wave has reached the sample, an impedance miss match between the sample and the rod (due to different modulus of elasticity) causes a portion of the wave to propagate through the specimen and a portion of the wave to reflect back from the interface of the rod and specimen. The wave that is reflected from the interface of the rod and specimen is known as the reflected wave. The wave passed through the specimen is known as the transmitted wave. The three stress waves induce a strain that can be measured using precision strain gages mounted at specified locations along the length of the incident and transmission bars. Strain rates varying from 100/s to 10,000/s can be achieved based on impact velocity, specimen size and geometry, and the mode of loading. Using the information obtained from the strain gages, stress versus strain graphs can be obtained. [27]

The Split Hopkinson Pressure Bar gives valuable information such as ultimate strength under dynamic loading conditions, stress versus strain for a dynamic loading case, strain to

ultimate failure, plastic strain, and energy absorption capacity. This information can then be compared to quasi-static loading. Using this comparison, information about increases or decreases in mechanical properties can be seen and used when modeling impact scenarios so that actual experimental testing can be minimized.

I.V Laser Occlusion Expansion Gage (LOEG)

The laser occlusion expansion gage is a newly developed apparatus designed as a non-contact way for obtaining sample strain under quasi-static and dynamic loading. Figures 1.18 and 1.19 show the LOEG setup.

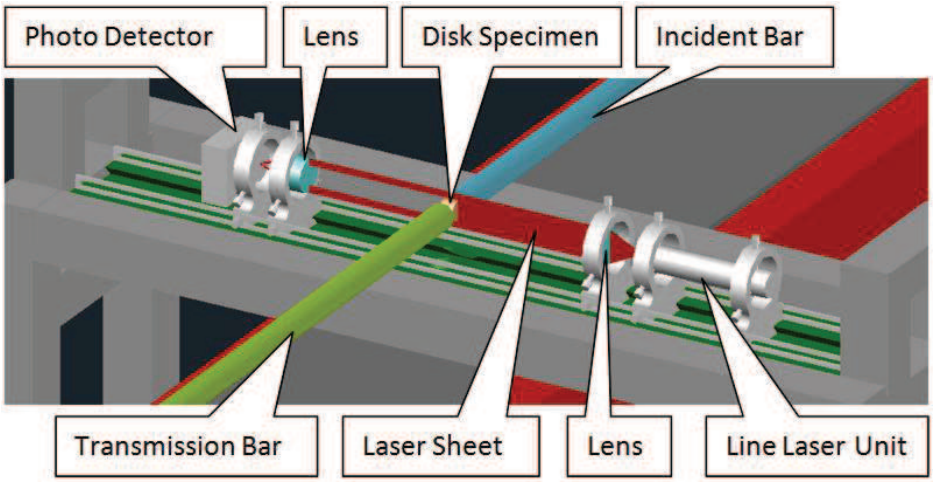

Figure 1.18 Laser Occlusion Expansion Gage Schematic [28]

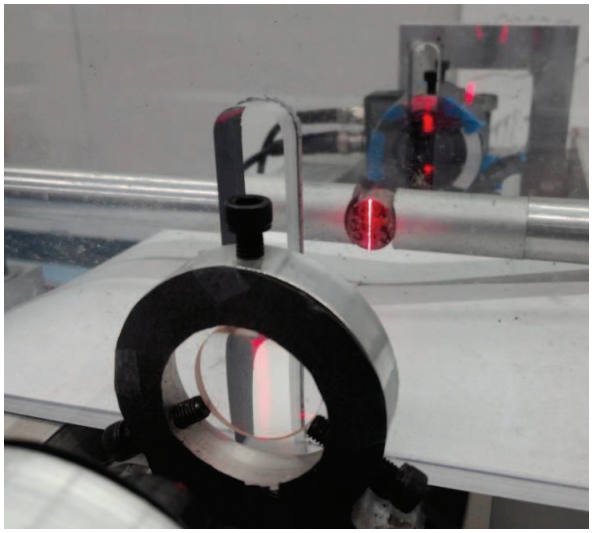

Figure 1.19 Laser Occlusion Expansion Gage (LOEG) Used for Experimental Data Collection [28]

The laser occlusion expansion gage uses a fanned laser. This laser is then focused into a sheet using a conical lens. This sheet then passes a sample which blocks a large portion of the emitted light. The light that is able to pass around the sample is then re focused into a photo detector which outputs a voltage signal based on the amount of light detected. The full field LOEG response with no sample present to block the focused laser sheet is approximately 1.25 volts. When a sample is placed inside the testing fixture the amount of light that is blocked is obtained from an oscilloscope. This drop in voltage will allow for a calibration factor of mV/unit of length. This calibration can then be used to calculate the strain in the sample during testing. The LOEG setup can be used to obtain global strains for compression test, direct tensile tests, and indirect tensile Brazilin disc tests.

During quasi-static and SHPB testing the deformation of the sample due to loading causes the sample to block more or less light depending on the setup. Only the indirect tensile Brazilin disc testing setup was used in this report. A schematic showing the Brazilian disc setup can be seen in Figure 1.20.

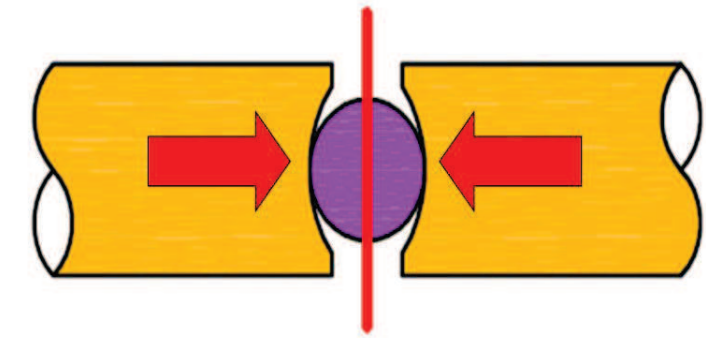

Figure 1.20 Indirect Tensile Laser Occlusion Expansion (LOEG) Gage Brazilian Disc Setup Schematic [28]

As the sample is loaded in compression the vertical axis expands causing more of the light to be blocked causing a drop in the signal response. This drop in signal can then be used to obtain strain, and strain rate data for both quasi-static and SHPB responsive of materials. The advantage to using the LOEG is that it is a non contact setup. This non contact setup allows and infinite amount of testing to be done without applying a strain gage directly to a sample, to acquire strain information that ultimately destroys the strain gage after testing. The LOEG was attempted to gather strain data for these brittle cementitious materials, without much success due to the small amount of strain causing failure of these materials.

CHAPTER II. METHODOLOGY

II.I Preparation of Materials

The metakaolin used was manufactured by calcinations of kaolinite at temperatures of approximately 800 °C. The metakaolin has a chemical composition of 96.8% amorphous composition, 2.2% quartz (SiO2), and 1.0% Anatase (TiO_2). An alkaline activator solution was prepared as a mixture of 15 M Na_2SiO_3 solution prepared by Sigma-Aldrich [29], and a 10 M solution of NaOH. The NaOH was prepared by mixing NaOH pellets from Sigma-Aldrich [30] with deionized water until a 10 M solution was formed. The Na_2SiO_3 and NaOH were then mixed thoroughly with an automated stirring rod for a minimum of 6 hours to ensure consistency. Using a 50:50 mix ratio the metakaolin was combined with the solution. The gel was then placed into 2 inch square cubes and a 10.16 cm x10.16 cm x 30.48 cm form. The forms were then placed in a moist environment for 24 hours. The forms were removed and placed inside plastic bags with wet paper towels and sealed. The bags were then placed inside an oven and heat cured using a 10 ˚C per 20 minute intervals and then held at 80 ˚C for 24 hours and cooled using the reverse heating cycle. This ramped heating and cooling cycle helped to minimize cracking due to thermal stresses [31]. Samples with a diameter of 16 mm and aspect ratio of 0.5, 0.75, 1.0, and 2.0 were cored from the cured metakaolin based geopolymer. 101.6 mm x 101.6 mm x 12.7 mm and 101.6 mm x 101.6 mm x 6.35 mm plates were cut using a wet saw.

The fly ash-based mortar was prepared from Class F fly ash produced at Tennessee Valley Authority coal-fired power plant at Cumberland City, TN, USA mixed with ASTM C 778

[32] graded quartz sand aggregate (U.S. Silica Ottawa, IL) [33]. The fly ash based geopolymer was prepared by mixing 51.74 wt % fly ash, 30 wt % sand, 13.04 wt % Na2SiO3, and 5.21 % 14 M NaOH [1]. The NaOH and the mixed Na_2SIO_3 and NaOH solution were prepared in the same manner previously stated. The solid and liquid mixture were mixed in a Hobart mixer and placed in a mold in two lifts and vibrated during both lifts. The fly ash was cured in a moist environment for 24 hours and then placed inside a plastic bag that contained wet paper towels and then placed in an oven set to a temperature of 40 ˚C for 48 hours. Samples were cut with the same dimensions as previously stated.

The Portland cement-based mortar having a water to cement ratio of 0.485 was prepared in accordance with ASTM C109/C109M-12 [34] and was used as a baseline for comparison. The Portland cement was cured inside a fog room for 96 hours before being demolded and cut to the sample sizes previously stated. Table 1-3 show the mix proportions of the 3 mortar systems tested.

Table 2.1 Portland Cement-Based Mortar Mix Composition

Portland Cement-Based Mortar Composition [34]

	Cement wt.%	Sand wt.%	Water wt.%
50% wt.%	23.62	64.95	11.43

Table 2.2 Metakaolin Geopolymer Mix Composition

Metakaolin Composition [1]

	Metakaolin wt.%	Sodium Silicate, PQ, D-51, wt.%	Sodium Hydroxide (14 M), wt.%
50% wt.%	50	25	25

Table 2.3. Fly Ash-Based Mortar Mix Composition

Fly Ash-Based Mortar Composition [33]

	Fly Ash, wt.%	Sodium Silicate, PQ, D-51, wt.%	Sodium Hydroxide (14 M), wt.%	Sand, wt.%
Mortar - 30%	51.74	13.04	5.21	30

II.II Specimen Preparation

This section will explain in detail how each sample was prepared and the reason why they are prepared in a specific manner.

II.II.I SEM, EDS, and Nanoindentation

SEM, EDS, and nanoindentation specimens were made by coring 16 mm diameter cylinders from large forms. After coring, samples and epoxy were placed inside a 32 mm diameter cylinder and left to set for 24 hours. Upon removal of mold a thin slice of the disc was cut to expose the surface of the sample using a precision wafering saw. Exposed samples were polished for 2 min at 120 rpm using 240 grit (51.8 μm), 400 grit (24.6 μm), 600 grit (14.5 μm), 1200 grit (6.5 μm), 0.3 μm alumina suspension, and 50 nm alumina suspension. Between each polishing step an optical microscope was used to measure crack width. If measured crack length was greater than the grit size the polishing step was repeated for that specific grit. [33]

II.II.II XRD

XRD samples were made by taking a small crushed sample of cured material for each mixture and using a 45 μm sieve until 90% pass rate was achieved. The sieved sample was then place in a random packed XRD sample holder.

II.II.III TGA

Thermo gravimetric analysis samples were prepared by crushing cured samples of each mixture until a fine powder was achieved.

II.II.IV Quasi-static, and SHPB

Quasi-static and SHPB specimens were made by coring out 16 mm diameter cylinders from larger forms. The samples cut using a precision wafering saw to give a thickness to diameter aspect ratio of one.

II.III Test Methods

This section will explain in detail the test methods used to acquire data for analysis.

II.III.I SEM and Optical Microscope

An FEI Nova NanoSEM 630 field emission SEM imaged the samples. Imaging was performed at an accelerating voltage of 10kV using a backscattered electron detector to reveal changes in microstructure and the presence of microcracking. Varying magnifications were used for each material. A Ziess Image.Z1m microscope equipped with an AxioCam MRc5 camera

was used to observe the distribution of aggregates at higher length scales using bright field reflective imaging.

II.III.II EDS

EDS samples were placed inside the SEM apparatus with the same parameters as previously stated. Using the EDS software images from the SEM were used for EDS analysis by selecting points, lines, and areas of the images and collecting chemical composition data.

II.III.III XRD

XRD patterns were obtained from an X'Pert Pro XRD using Co K-α Radiation. The X-Ray patterns were obtained from 2 ˚to 70 ˚ 2θ with a scan rate of 0.57 ˚ 2θ/ min. The step size was <0.02 ˚.

II.III.IV TGA

TGA samples were placed inside a crucible of known weight. The crucible was placed on the STA 449 F1 Jupiter Thermo Gravimetric Analysis Machine stage. The samples were placed in a temperature and atmospheric regulated chamber by the machine. The purge was set to 50 ml/min and the protection was set to 20 ml/min. The temperature rate of changes was set to 10 °C/min starting from 35 °C and elevating the temperature to 1000 °C in a nitrogen atmosphere.

II.III.V Nanoindentation

The MTS Nano Indenter G200 was used to make small indentation on the surface of the materials to obtain modulus of elasticity and hardness values. 500 indents were done with a 50 x 10 grid arrangement. The spacing between the indents is 10μm and 20μm on the horizontal and vertical axis, respectively. A sample load rate of 0.2 mN/s with a maximum load of 2 mN was used. A 5 s hold time and a 10 s unload time was used.

II.III.VI Quasi-Static Compression

Quasi-static compression tests were done in accordance with ASTM C469-02 [35]. Compression loading rates of 241 ± 34 kPa (35 ± 5 psi)/s were used. Cord modulus of elasticity, 40% of compressive failure stress, axial strain at 40 % of compressive failure stress, and ultimate compressive stress data was recorded.

II.III.VII Quasi-Static Indirect Tension

Quasi-static tensile testing was done on a Enduratec SmarttestSP-AT machine. Using a curved fixture Brazilian disc test was conducted at a loading rate of 0.01 mm/sec. Load data was collected using Bose WinTest 4.1 program, and strain data was collected using Laser Expansion Gage (LEG). The specimen size used have a diameter of 16 mm nominal and an aspect ratio of one.

II.III.VII Low-Velocity Impact

Low-velocity impact tests were done on a Dynatup test machine. Due to the lack of a standard for testing cement materials under low-velocity impact situation ASTM D3763-10 [36]

was used to guide the formulation of a proper testing setup. A mass of 3.32 Kg was dropped from a height of 22.04 cm. Load and displacement data were collected and processed by Dynatup Impulse Data Acquisition Software [37].

II.III.VIII Split Hopkinson Pressure Bar

Using an aluminum SHPB apparatus, high strain rate testing was done for compression, and indirect tension. All tests were performed using a reservoir pressure of 8 psi and 4 psi, for compression and indirect tension test respectively, to launch the striker bar. Strain gage data was used to obtain stress and strain information using conventional SHPB theory equations for compression test. Using a Laser Occlusion Expansion Gage [28] strain data was collected and compiled with stress data obtained from strain gages on the bar for tensile specimens only.

CHAPTER III. RESULTS AND DISCUSSION

III.1 SEM

It was observed that the cement paste region of the Portland cement based-mortar has areas of un-hydrated cement. Figures 3.1 – 3.3 show SEM analysis images of the Portland cement-based mortar, and crack propagation around un-hydrated cement.

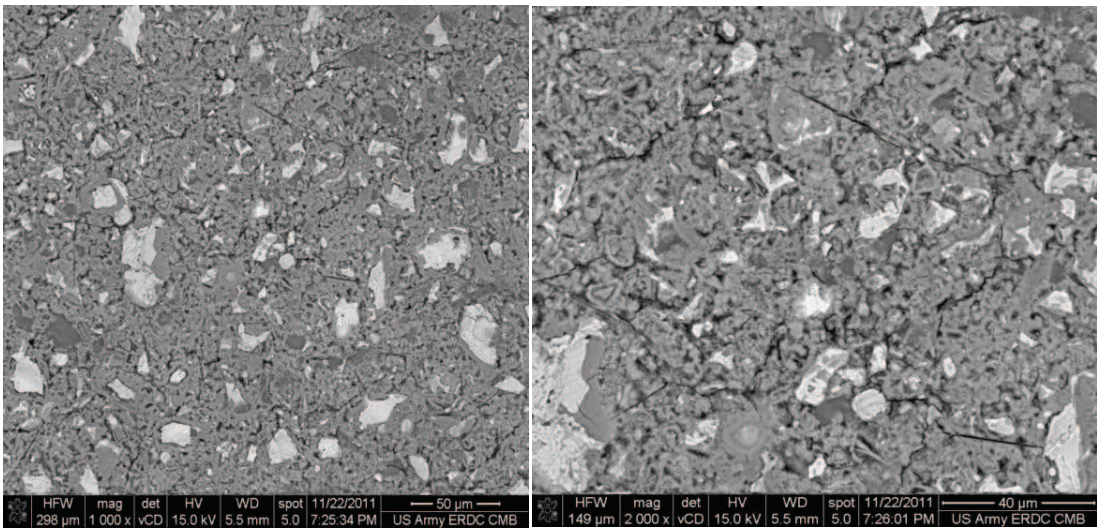

Figure 3.1 Scanning Electron Microscope Images of Portland Cement-Based Mortar

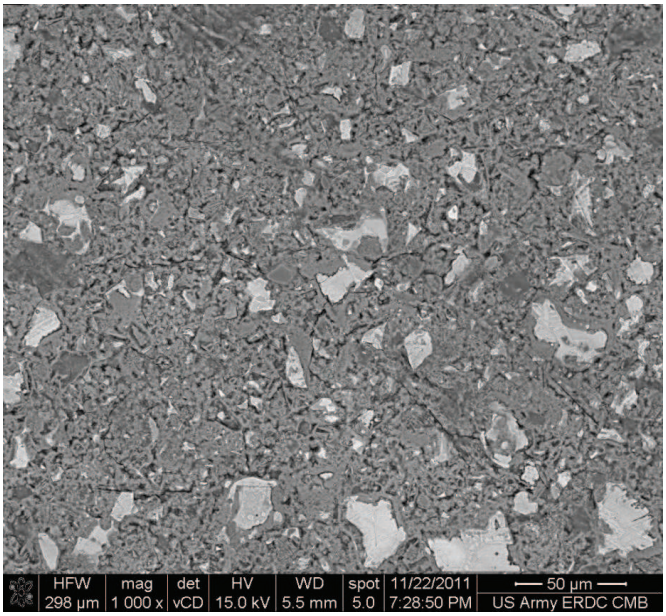

Figure 3.2 Scanning Electron Microscope Image of Portland Cement-Based Mortar Location 2

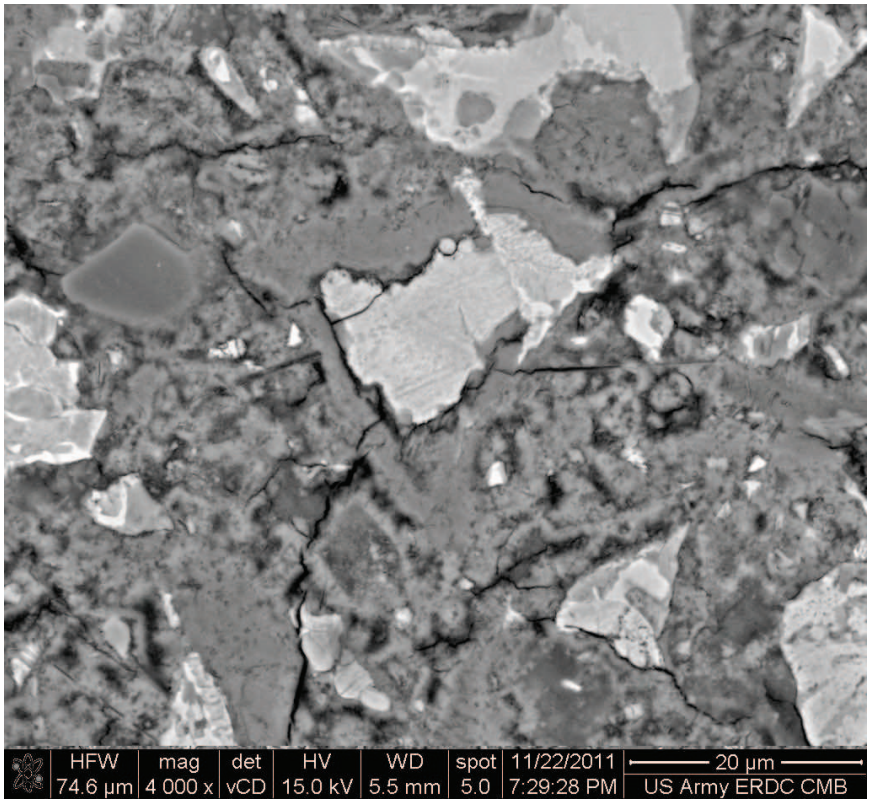

Figure 3.3 Micro Crack Propagation through Portland Cement-Based Mortar

It was observed that the crack followed a path near and around non reacted Metakaolin which may be due to diminished mechanical properties around the non reacted Metakaolin. Figures 3.4- 3.6 shows typical SEM image of metakaolin, cracks emanating from voids and non reacted metakaolin, and micro crack propagation.

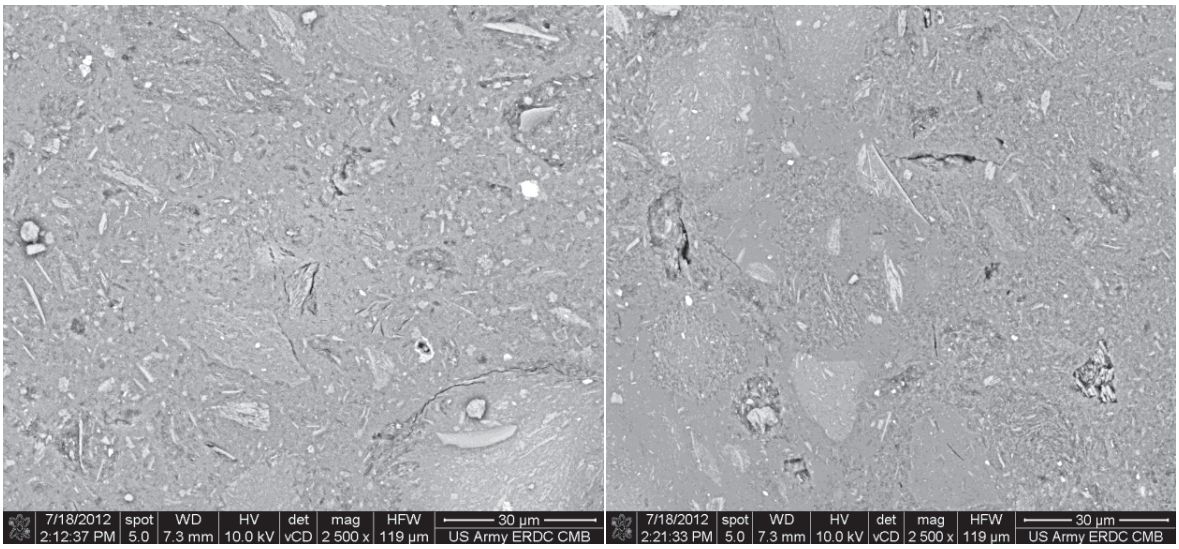

Figure 3.4 Scanning Electron Microscope Images of Metakaolin

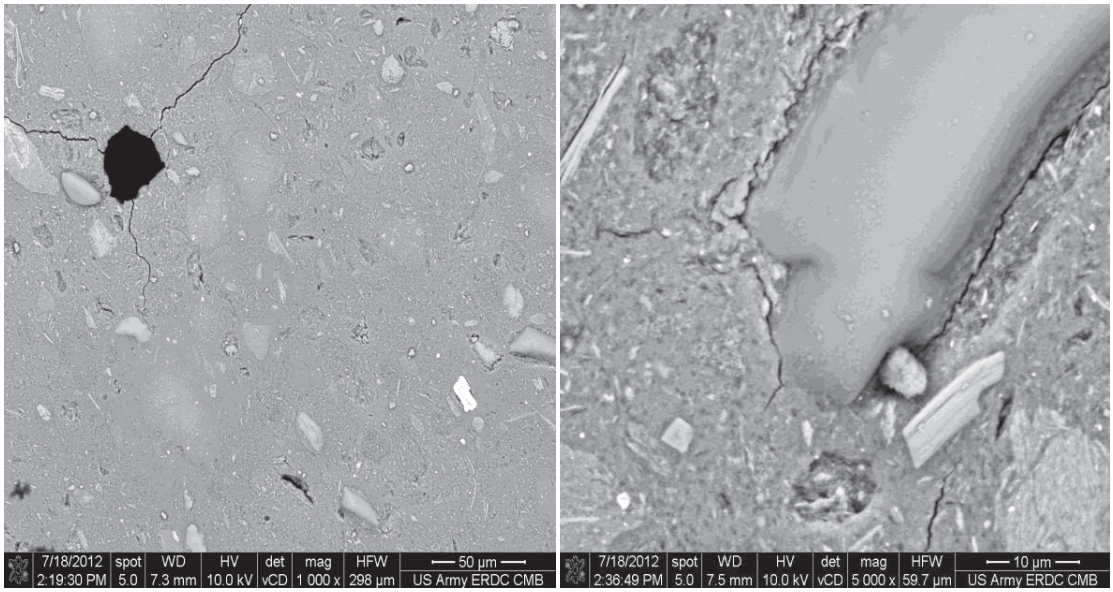

Figure 3.5 Crack Emanating from voids and Non Reacted Metakaolin

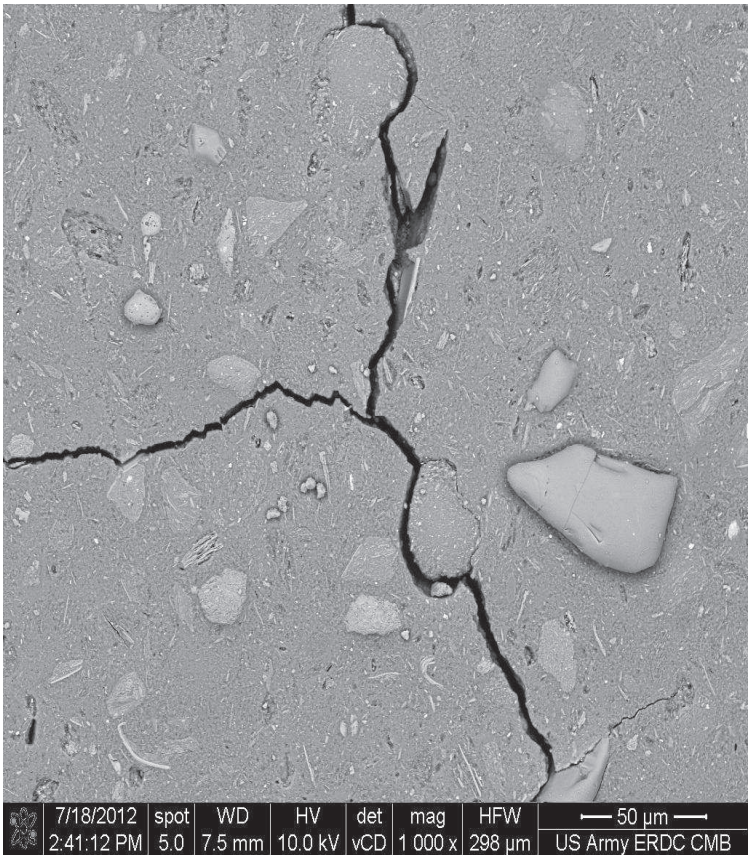

Figure 3.6 Micro Crack Propagation through Metakaolin

The SEM images for class F fly ash-based mortar show un-reacted class F fly ash-based mortar, and Hematite crystals. Figure 3.7 – 3.9 show typical SEM images of the class F fly ash-based mortar.

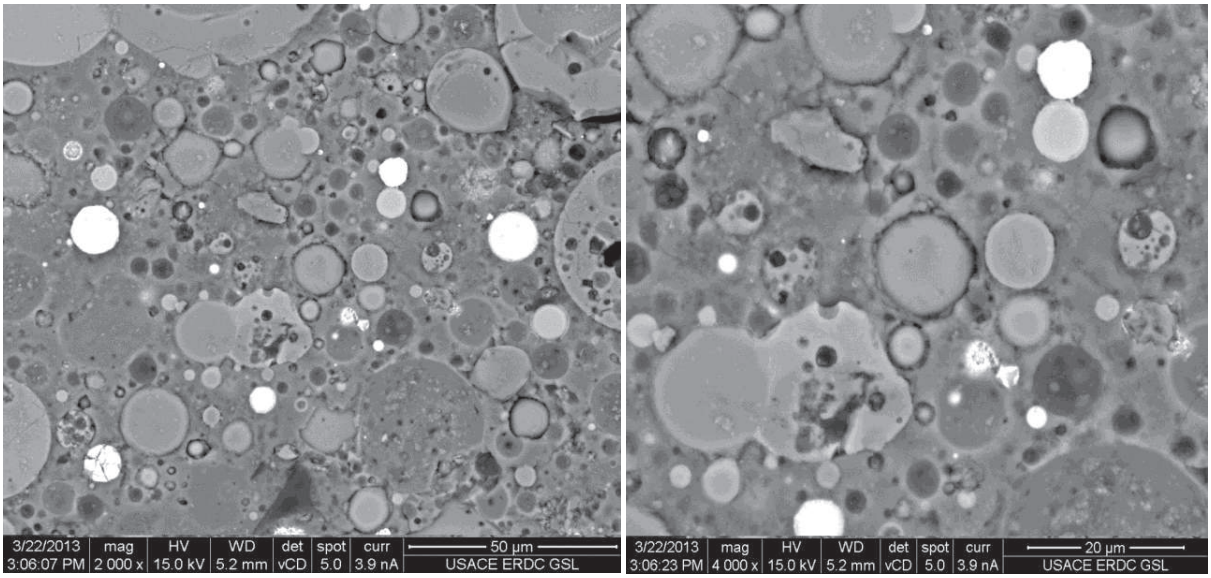

Figure 3.7 Scanning Electron Microscope Images of Class F Fly Ash-Based Mortar

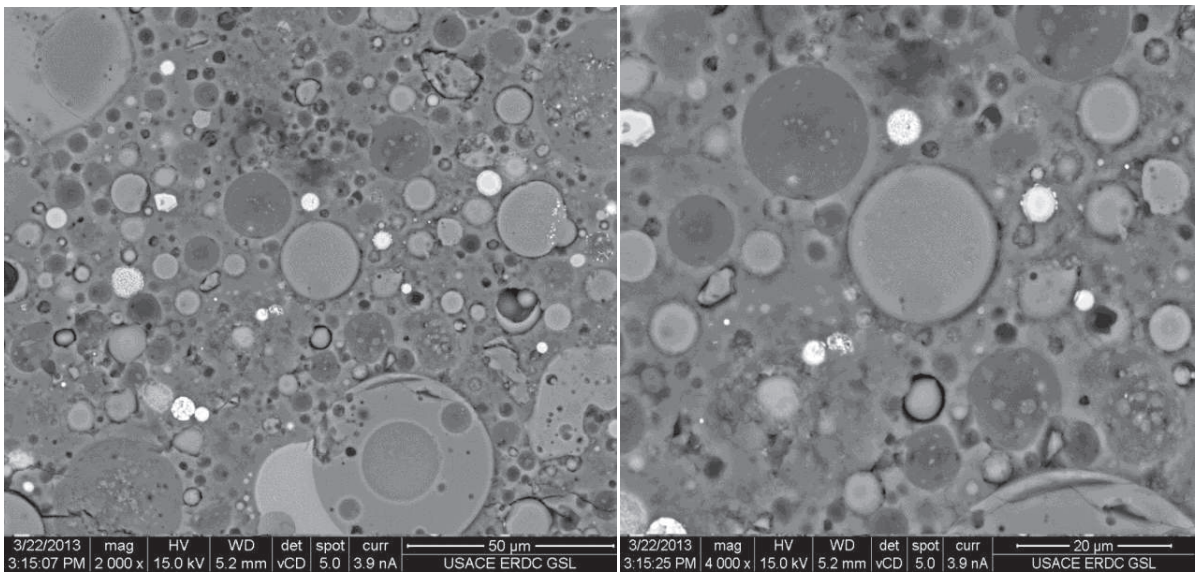

Figure 3.8 Scanning Electron Microscope Images of Class F Fly Ash-Based Mortar Location 2

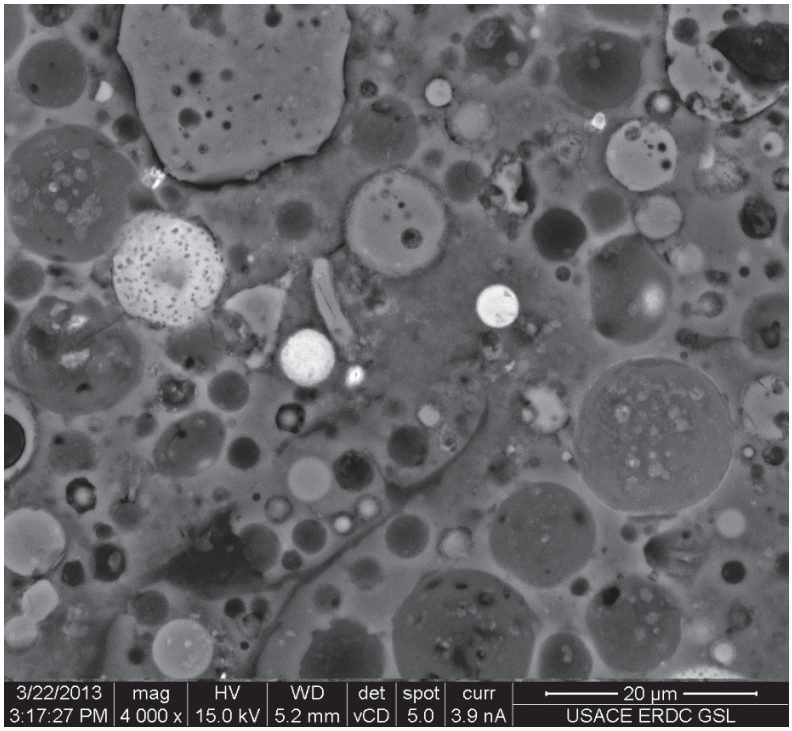

Figure 3.9 Scanning Electron Microscope Images of Class F Fly Ash-Based Mortar Location 3

III.II EDS

Due to the unavailability of the EDS equipment at the time of imaging the Portland cement-based mortar EDS analysis of the Portland cement-based mortar will not be presented.

The EDS analysis shows the elemental composition of the cementitious materials. SEM images coupled with EDS tabular elemental composition was done at 4 different locations for Metakaolin. Figure 3.10 - 3.17 shows the EDS location and corresponding EDS signals for Metakaolin. Tables 3.1 – 3.4 shows a tabular elemental composition.

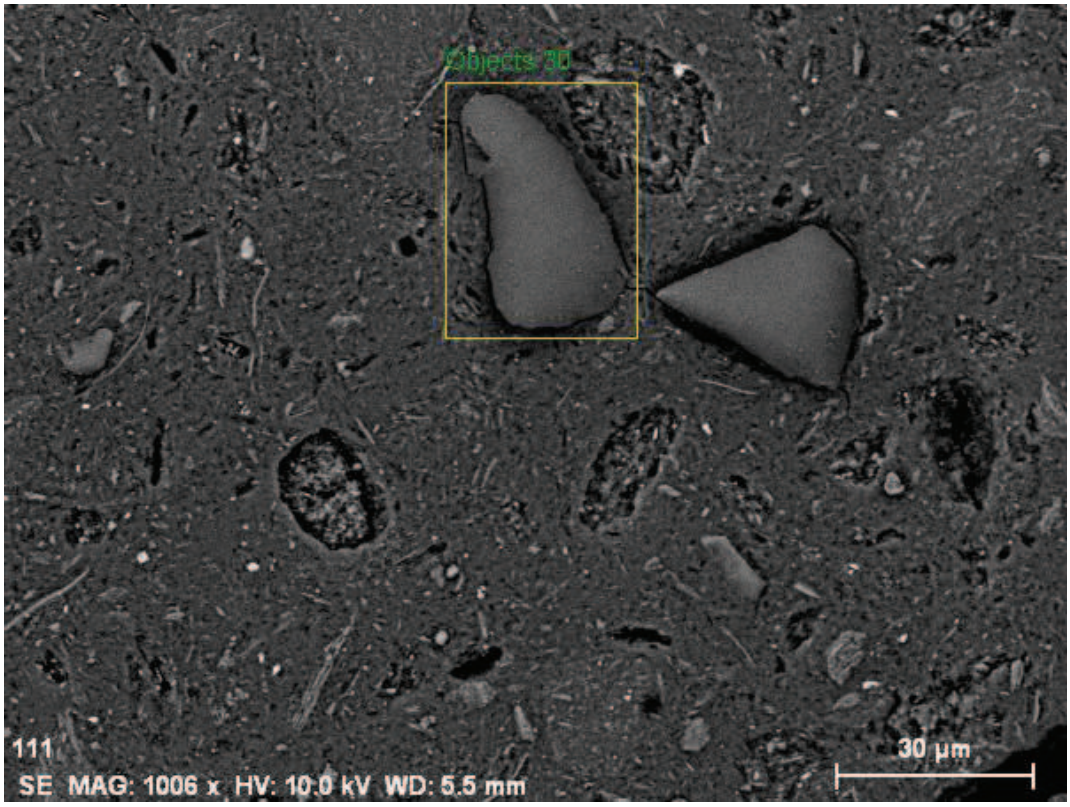

Figure 3.10 Energy Dispersive Spectroscopy Image Object 30

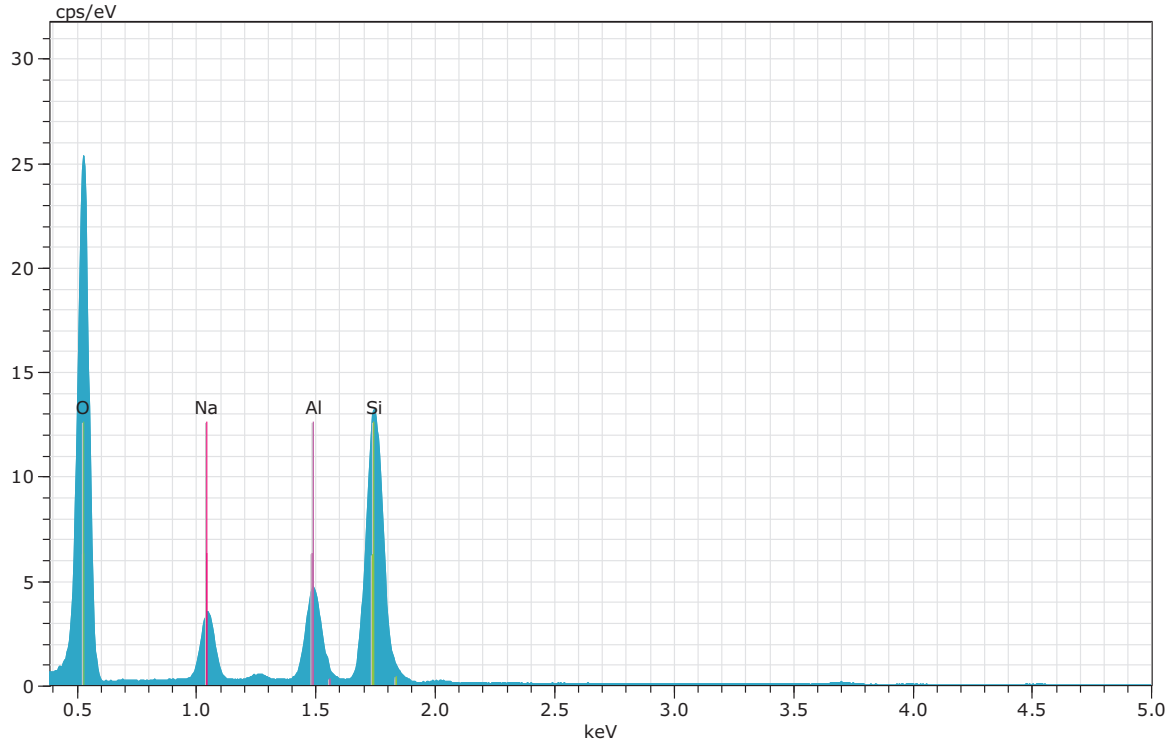

Figure 3.11 Energy Dispersive Spectroscopy Spectrum Object 30

Table 3.1 Object 30 Spectrum

El	AN	Series	unn. C [wt.%]	norm. C [wt.%]	Atom. C [at.%]	Error(1 Sigma) [wt.%]
O	8	K-series	56.43	57.12	68.80	6.36
Si	14	K-series	20.58	20.86	14.32	0.87
Al	13	K-series	12.49	12.66	9.04	0.59
Na	11	K-series	9.23	9.35	7.84	0.57
		Total:	112.23	100	100	

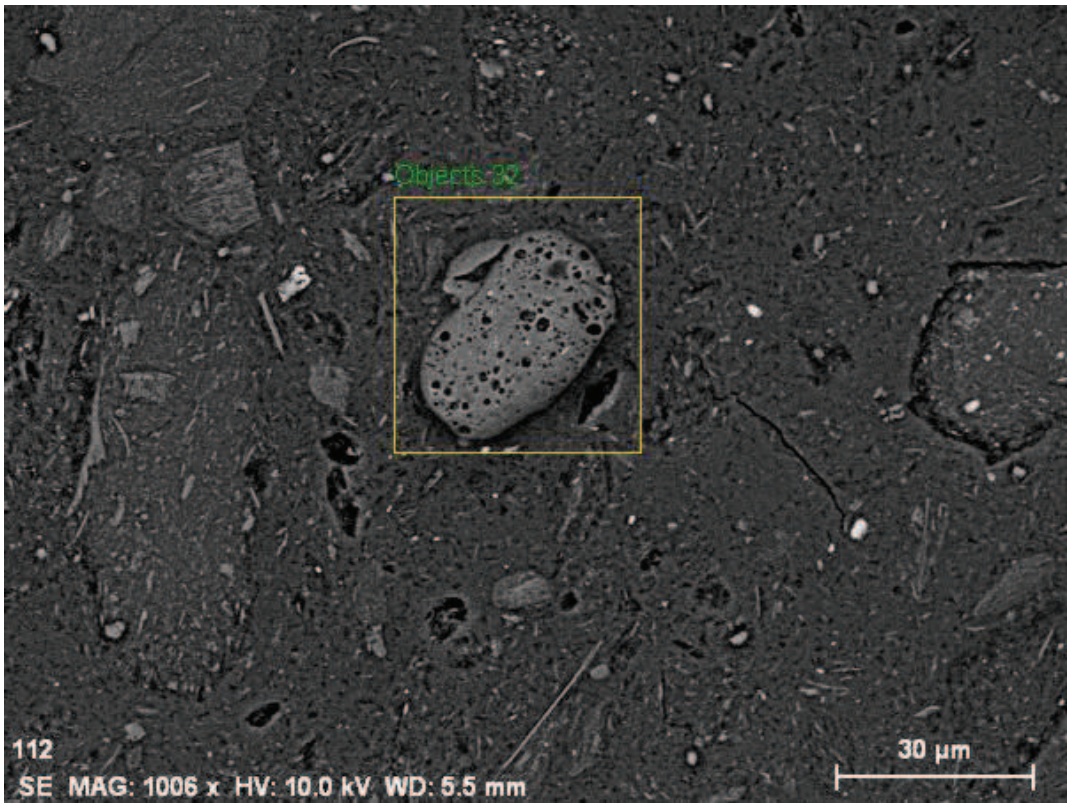

Figure 3.12 Energy Dispersive Spectroscopy Image Object 32

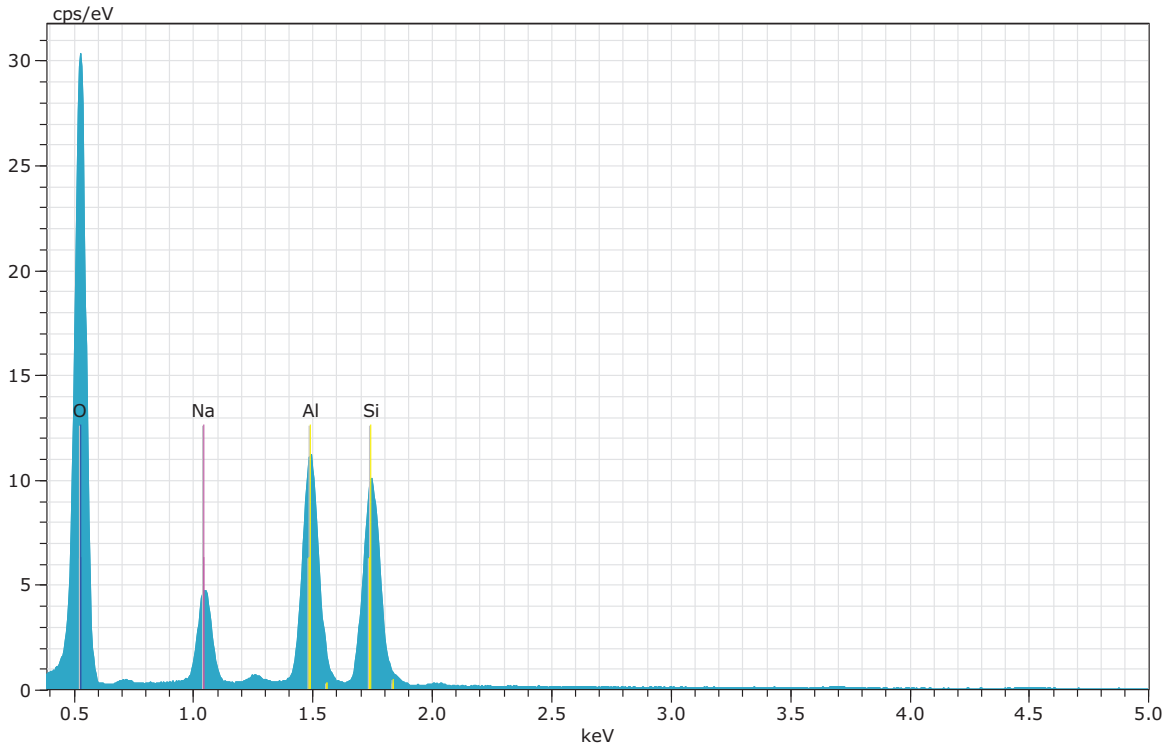

Figure 3.13 Energy Dispersive Spectroscopy Spectrum Object 32

Table 3.2 Object 32 Spectrum

El	AN	Series	unn. C [wt.%]	norm. C [wt.%]	Atom. C [at.%]	Error(1 Sigma) [wt.%]
O	8	K-series	55.07	55.63	67.80	5.99
Si	14	K-series	22.09	22.31	15.49	0.93
Al	13	K-series	15.84	16.00	11.56	0.74
Na	11	K-series	6.01	6.07	5.15	0.38
		Total:	99.00	100	100	

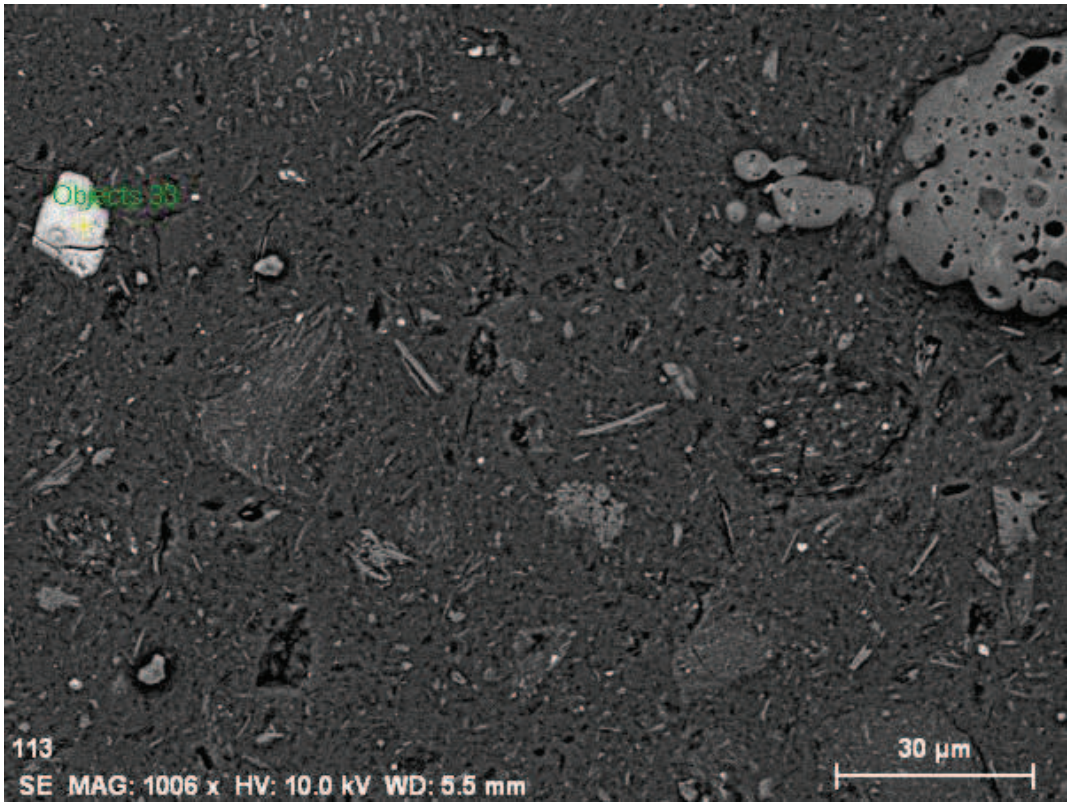

Figure 3.14 Energy Dispersive Spectroscopy Image Object 33

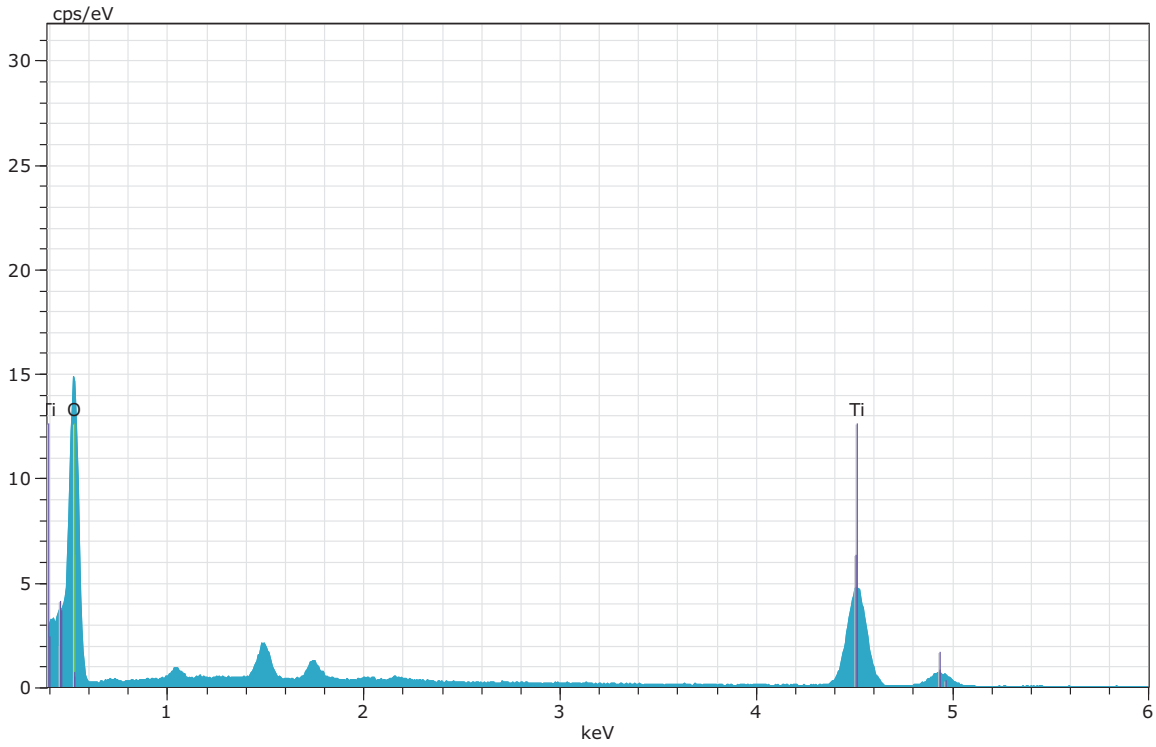

Figure 3.15 Energy Dispersive Spectroscopy Spectrum Object 33

Table 3.3 Object 33 Spectrum

El	AN	Series	unn. C [wt.%]	norm. C [wt.%]	Atom. C [at.%]	Error(1 Sigma) [wt.%]
O	8	K-series	38.40	40.90	63.26	4.61
Ti	22	K-series	51.73	55.10	28.48	1.83
C	6	K-series	3.76	4.01	8.26	0.64
		Total:	93.89	100	100	

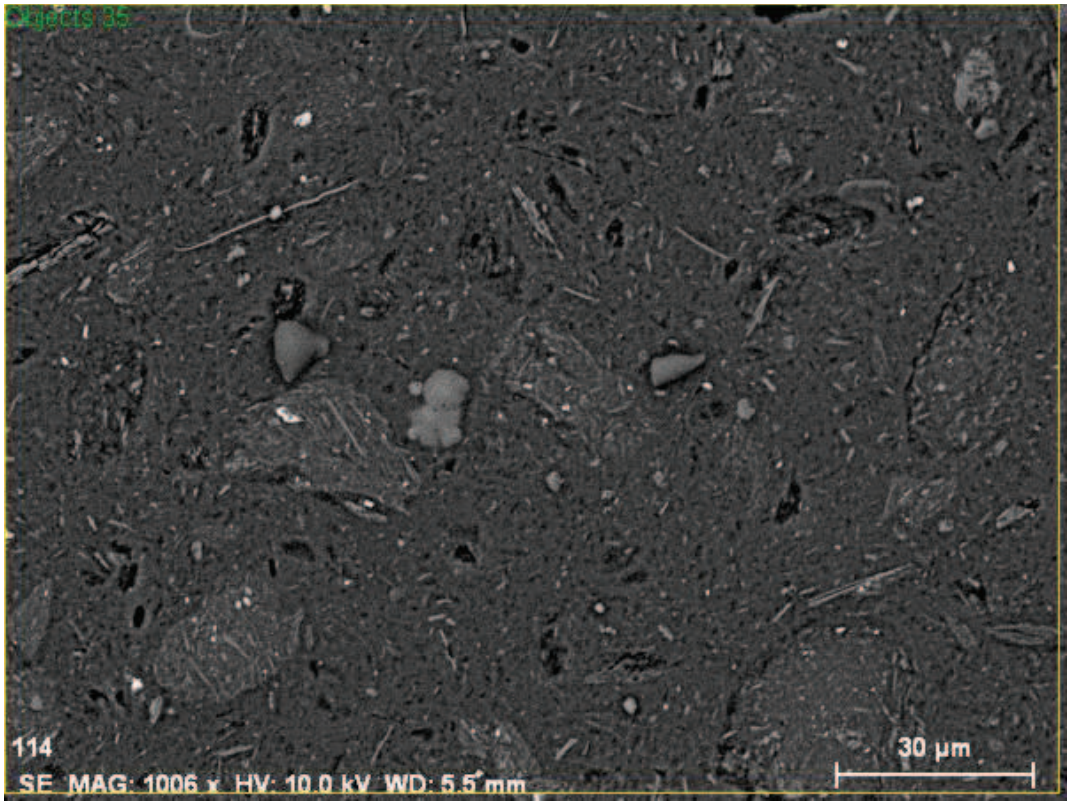

Figure 3.16 Energy Dispersive Spectroscopy Image Object 35

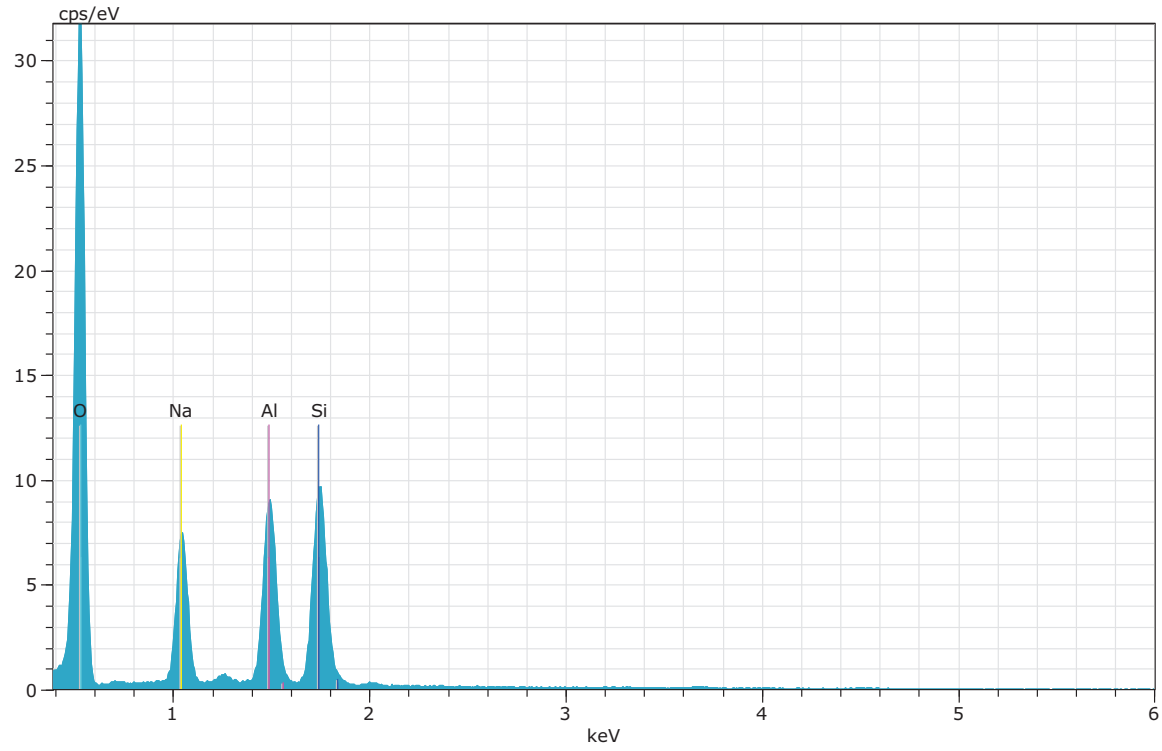

Figure 3.17 Energy Dispersive Spectroscopy Spectrum Object 35

Table 3.4 Object 35 Spectrum

El	AN	Series	unn. C [wt.%]	norm. C [wt.%]	Atom. C [at.%]	Error(1 Sigma) [wt.%]
O	8	K-series	56.34	57.12	68.80	6.36
Si	14	K-series	20.58	20.86	14.23	0.87
Al	13	K-series	12.49	12.66	9.04	0.59
Na	11	K-series	9.23	9.35	7.84	0.57
		Total:	98.64	100	100	

From the EDS results the elemental makeup of the metakaolin is Oxygen, Silicon, Aluminum, Sodium, Titanium, and Carbon. This result matches what would be expected from mixing reactants previously stated for metakaolin. The impurities of Titanium and Carbon are present in the EDS signals. This is collaborated by the Nanoindentation, and XRD results for metakaolin.

The EDS analysis of the class F fly ash shows the presence of sodium, aluminum, silicon, and calcium. Figure 3.18 shows the distribution of elements in the class F fly ash-based mortar.

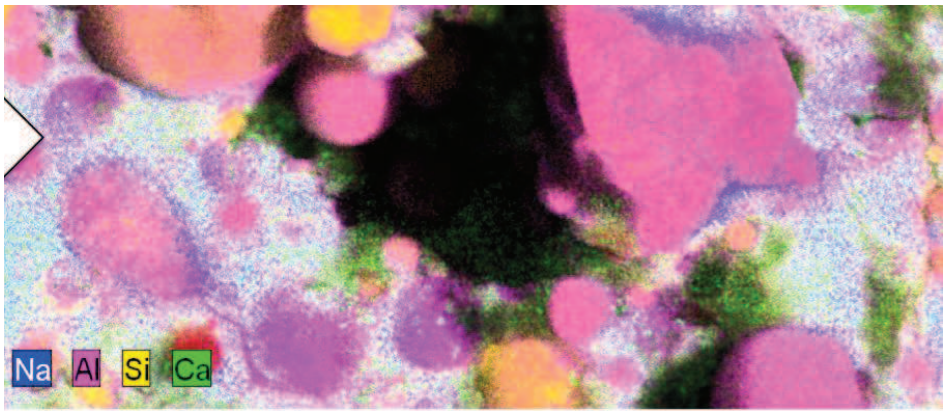

Figure 3.18 Energy Dispersive Spectroscopy Image of Class F Fly Ash-Based Mortar [33]

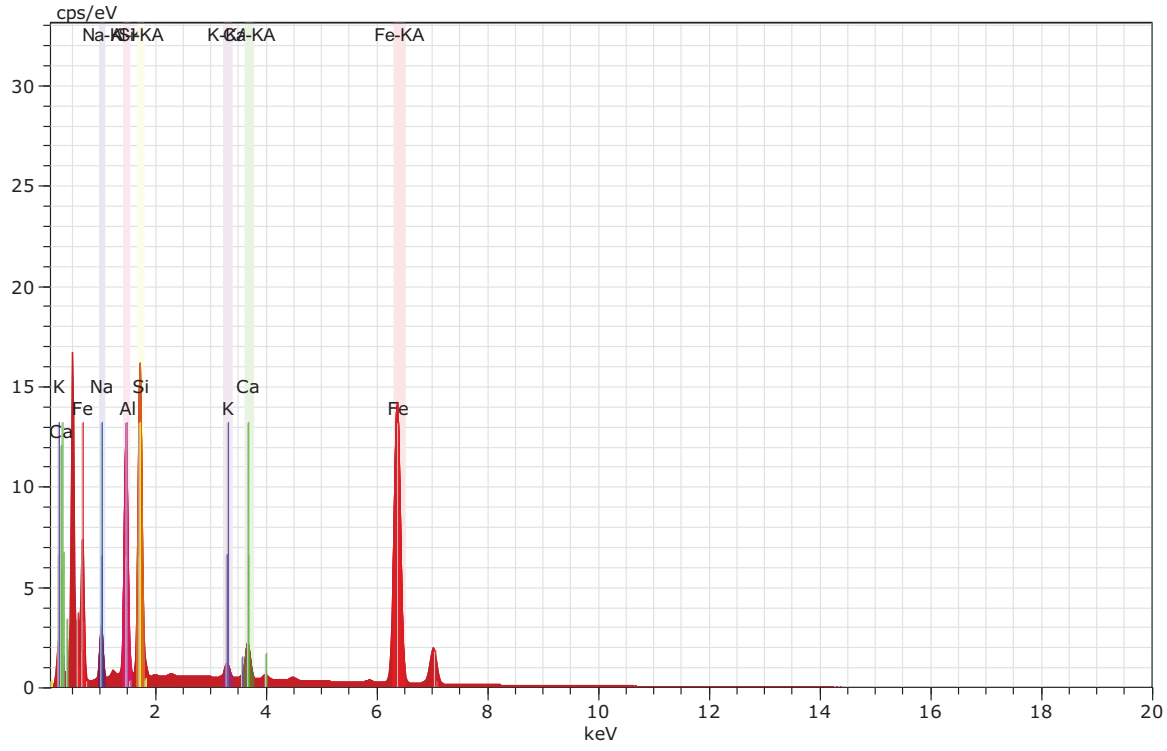

Figure 3.19 Eenergy Dispersive Spectroscopy Analysis of Class F Fly Ash-Based Mortar [33]

III. III XRD

The XRD patterns show in Figures 3.20 – 3.22 show the crystalline chemical composition for each material. There are 4 phases present in the Portland cement-based mortar. Quartz (SiO_2), Portlandite ($Ca(OH)_2$), Alite Monoclinic (Ca_3SiO_5), and Calcite ($CaCO_3$). This is what is expected in the Portland cement-based mortar that has sand as a fine aggregate. This information shows that no adverse chemical reactions took place. The metakaolin shows a large amorphous hill between 25 ˚ to 45 ˚ 2θ. It also shows two crystalline impurity structures Quartz (SiO_2) and Anatase (TiO_2), and is typically seen in metakaolin geopolymers. The class F fly ash-based mortar contained Quartz (SiO_2), Mulite ($Al_6Si_2O_{13}$), Calcite ($CaCO_3$), Magnetite ($Fe+2Fe_2+3O_4$), and Hematite (Fe_2O_3). This is typical for a class F fly ash-based mortar. The large amount of Quartz is due to the addition of sand as a fine aggregate. The other impurities could be due to debris and contaminates in the mixing procedure and is typical for a class F fly ash-based mortar.

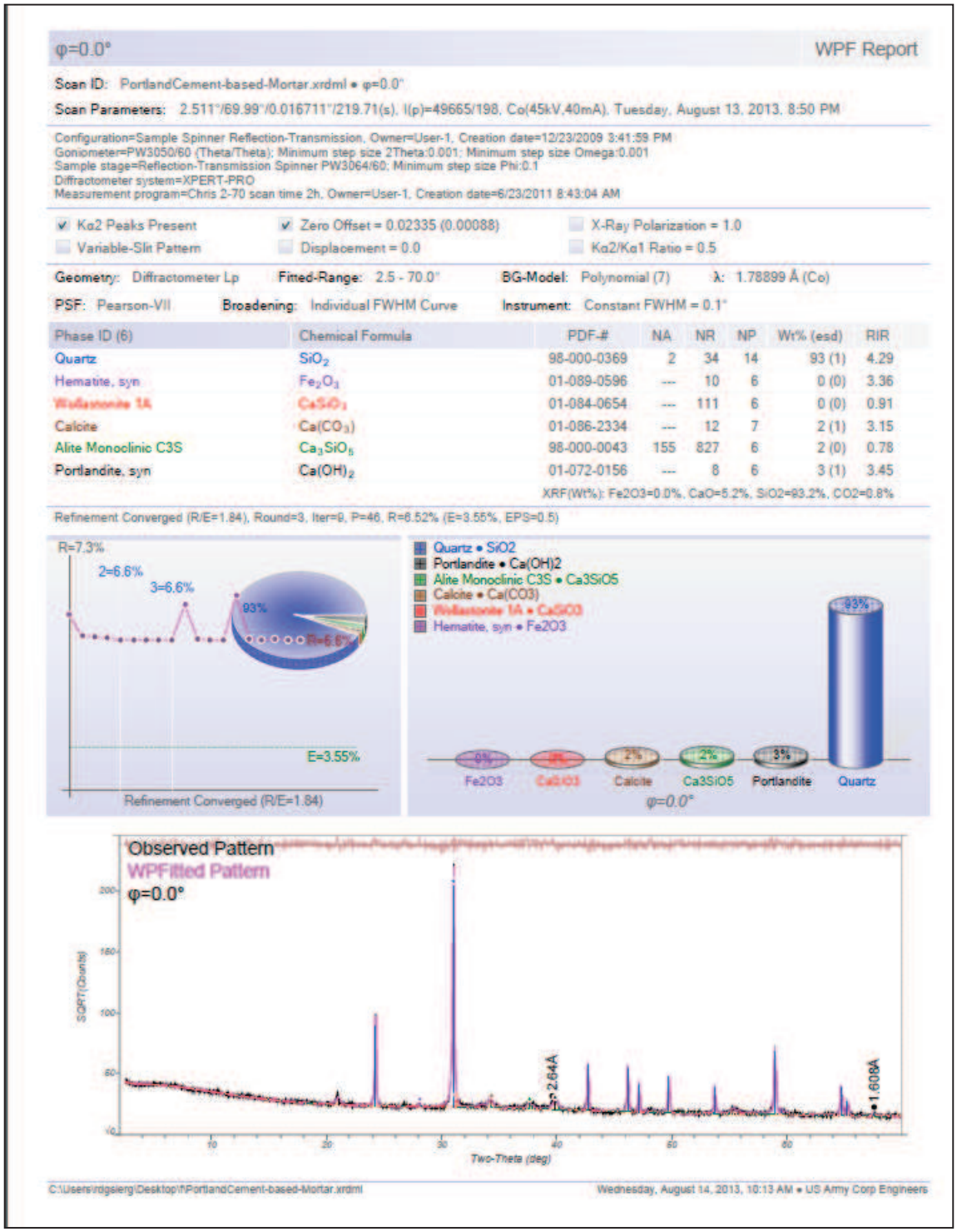

Figure 3.20 X-Ray Diffraction of Portland Cement-Based Mortar

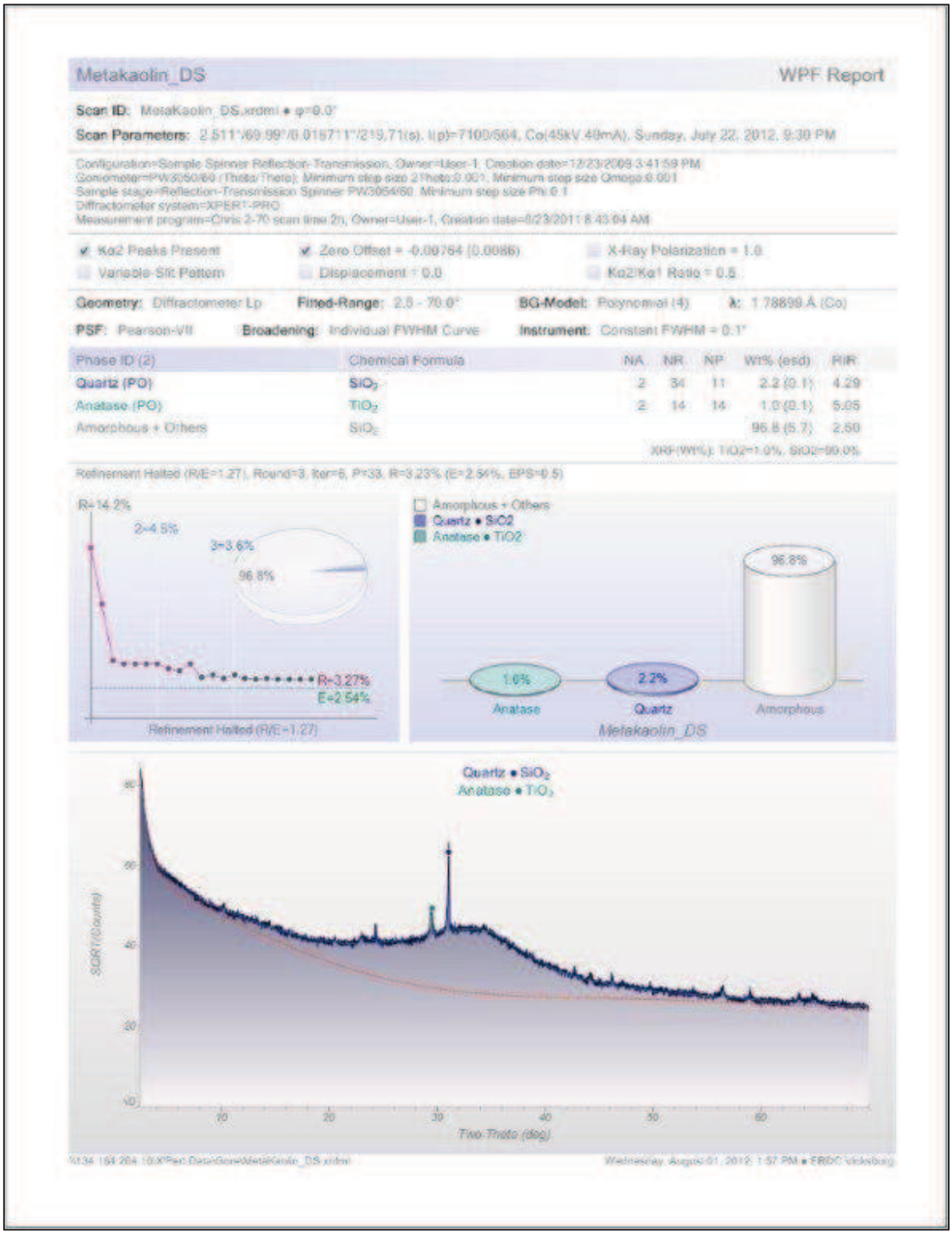

Figure 3.21 X-Ray Diffraction of Metakaolin

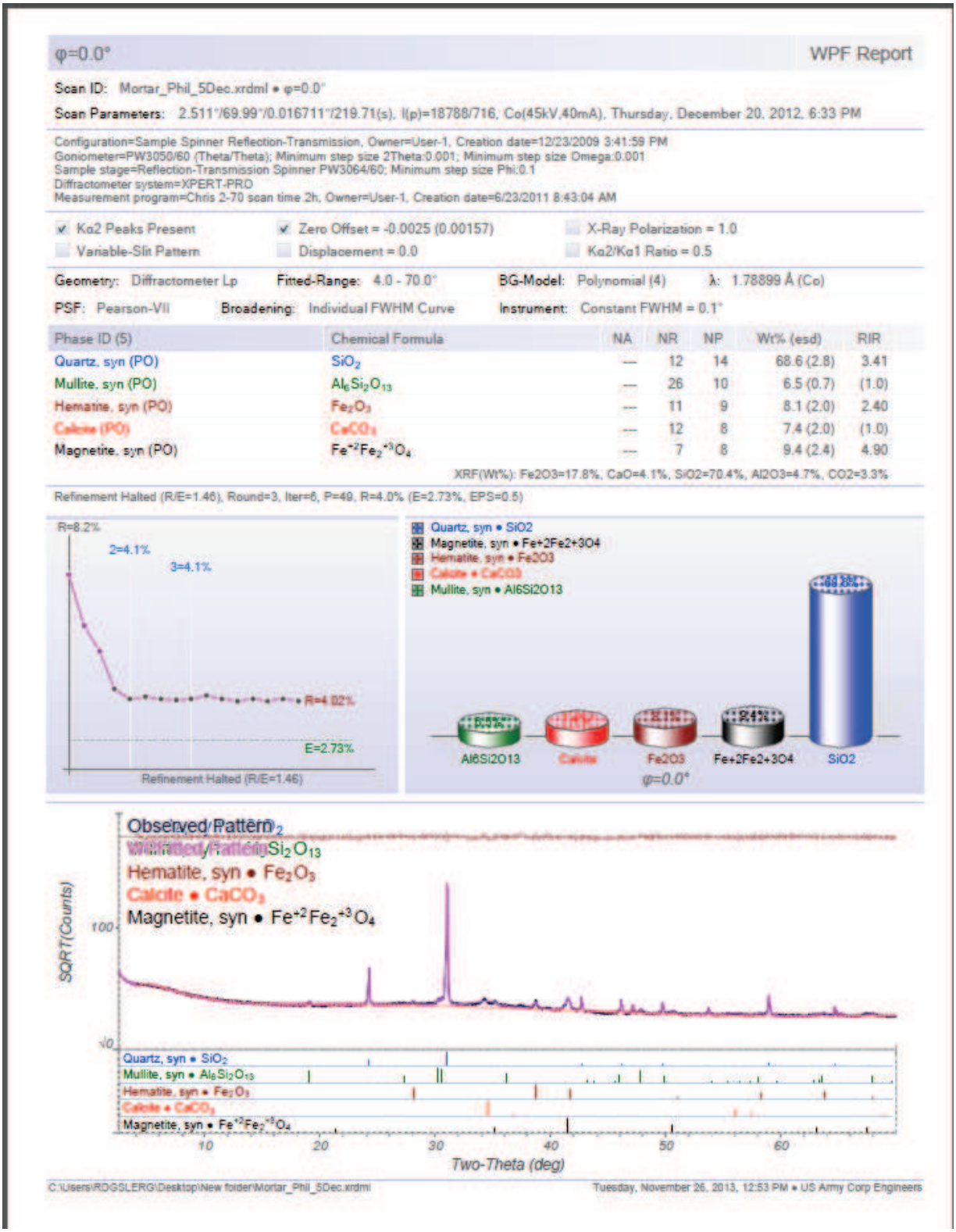

Figure 3.22 X-Ray Diffraction of Class F Fly Ash-Based Mortar

III.IV TGA

TGA was performed on two samples and the resulting information is displayed below in figures 3.23 and 3.24. There is a drastic weight loss between the start of the experiment to approximately 15 minutes. Since the rate of temperature change is 10 ˚C/min, the final temperature corresponds to approximately 185 ˚C. This weight loss is typically due to water. The TGA analysis show that there are only two phases present in the metakaolin geopolymer residual water that could have been present due incomplete heating during curing or absorbed moisture from the atmosphere during specimen preparation. Figures 3.15 and 3.16 also show that there may be a glass transition temperature around 870 ˚. This is consistent with published glass transition temperatures for metakaolin geopolymers.

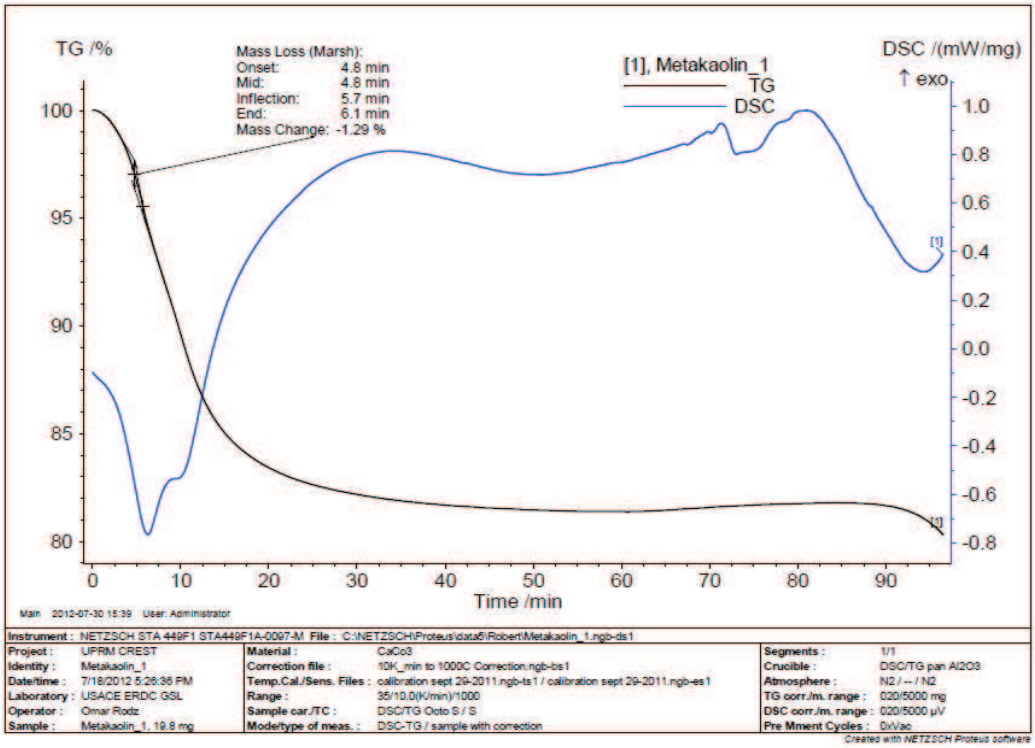

Figure 3.23 Thermo Gravimetric Analysis of Metakaolin Sample 1

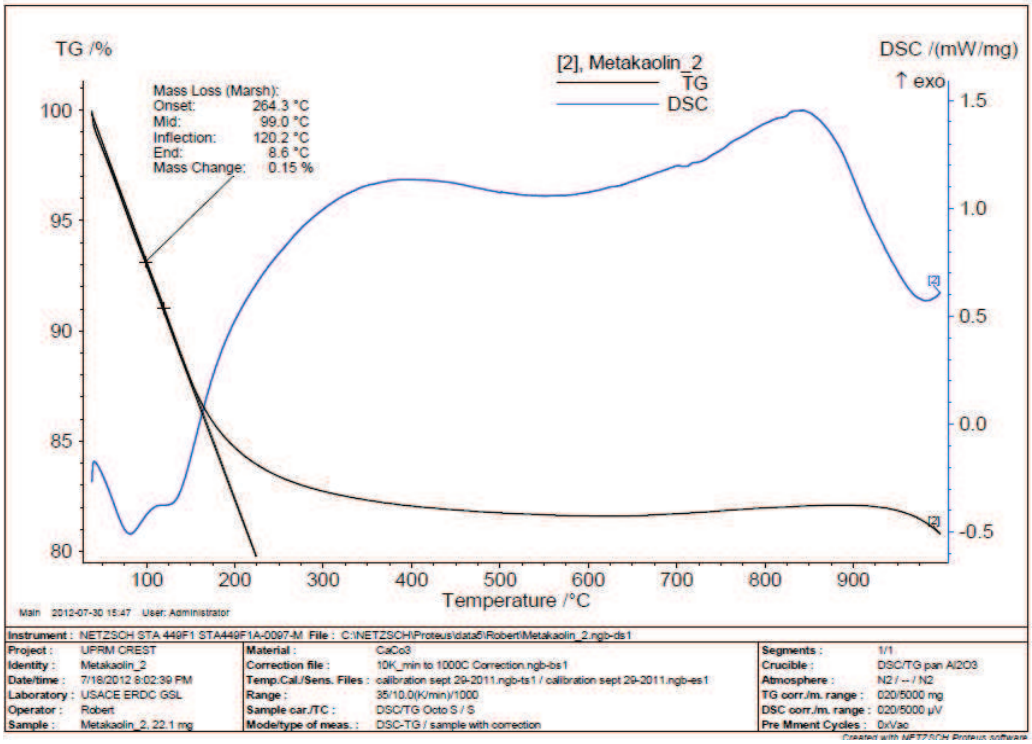

Figure 3.24 Thermo Gravimetric Analysis of Metakaolin Sample 2

III.V Nanoindentation

The modulus of elasticity of Metakaolin was derived from the 50 x 10 grid of nanoindentation. Statistical analysis of the 500 nanoindentions was done using STAT-17F from MIL-Handbook-17F [38]. This allowed the elimination of outliers in the nanoindention data for the elastic modulus and the hardness values. After elimination of outliers the calculated average modulus of elasticity was found to be 11.3 GPa with a standard deviation of 4.09 GPa. The average hardness value was found to be 0.518 GPa and a standard deviation of 0.214 GPa. The elastic modulus of Anatase, quartz, is 230 GPa, 70 GPa respectively. The far left load versus deflection plots in Figure 19 more than likely represent the Anatase the modulus of the graph is approximately 50GPa. The large difference in the expected value of the modulus of Anatase and the experimental value can be attributed to several reasons such as indention done on surface that

is not flat, cracking during the procedure, cracking of Metakaolin around the Anatase during test, and indention between two different phases. The middle load versus deflection plots more than likely represent the quartz present in the Metakaolin. The modulus of the two graphs on the far right is on average 25GPa. Differences in the expected modulus of quartz and experimental modulus of quartz can be attributed to the same reason stated for Anatase. The far left load versus deflection plots represents the Metakaolin modulus and on average was 11.3GPa. The occurrence of the 50GPa and 25GPa modulus was approximately 5-10 in the 500 nanoindents performed, which is the expected occurrence based on the XRD information. Typical nanoindent load versus displacement results are shown for Metakaolin in Figure 3.25.

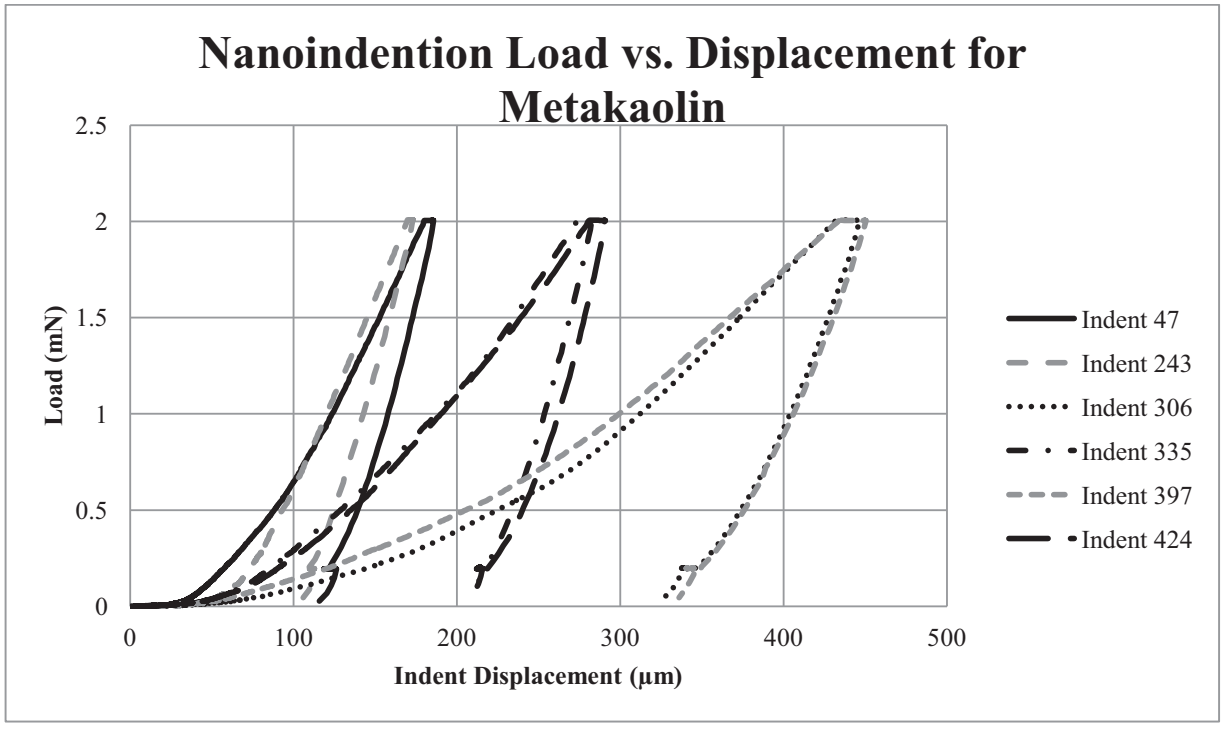

Figure 3.25 Load vs. Displacement from Nanoindentations of Metakaolin

The modulus of elasticity was obtained using the same grid pattern as previously stated. Figure 3.26 shows typical indents done on class F fly ash-based mortar.

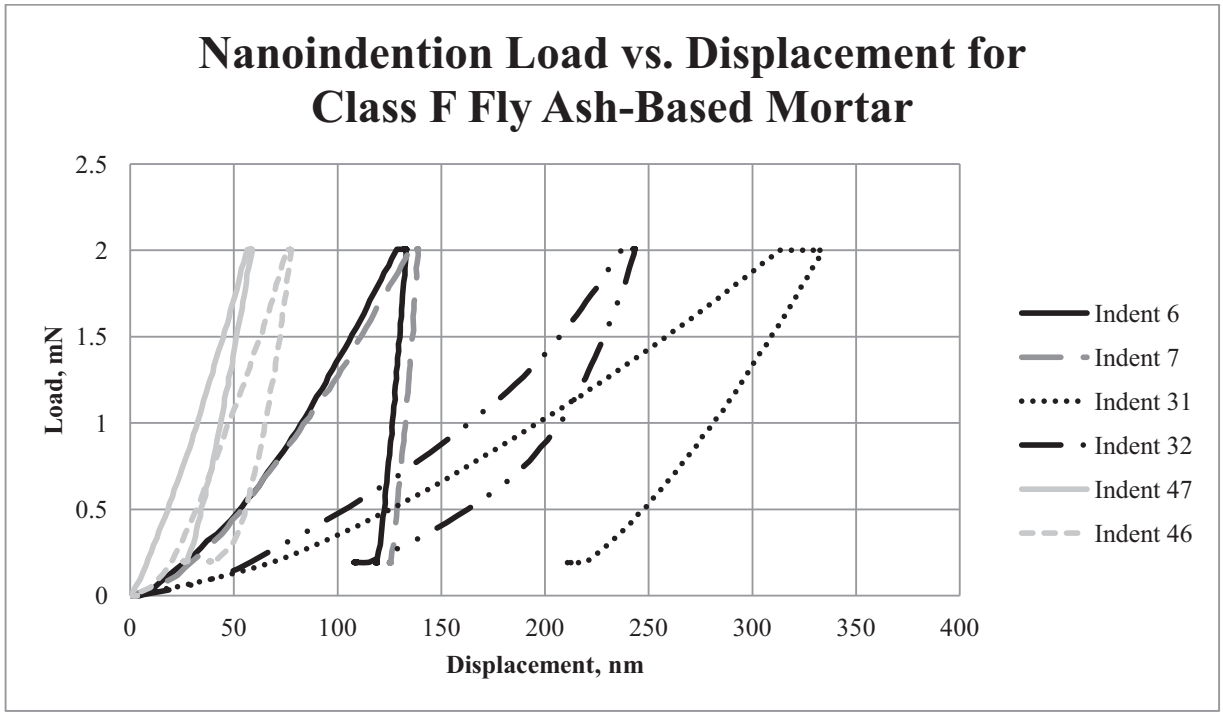

Figure 3.26 Load vs. Displacement from Nanoindentations of Class F Fly Ash-Based Mortar

The far right plots in figure yielded a modulus of 500 GPa possible due to indenting on a Hematite crystal. The middle plots yielded a modulus of 270 GPa possible due to indention on a magnetite crystal. The far left indents plots have a modulus of 20 GPa which is consistent with a class F fly ash-based mortar paste region.

III.VI Quasi-Static Compression

Three samples were used to collect ultimate stress data from quasi-static compression test samples. Graphical plots of the data collected show that the Portland cement-based mortar had the highest ultimate stress under quasi-static loading condition. Figure 3.27 shows stress versus strain data for the 3 cementitious materials analyzed in this report. Figure 3.28 shows the ultimate strength of each material with appropriate scatter bands for the 3 samples tested for each

material.

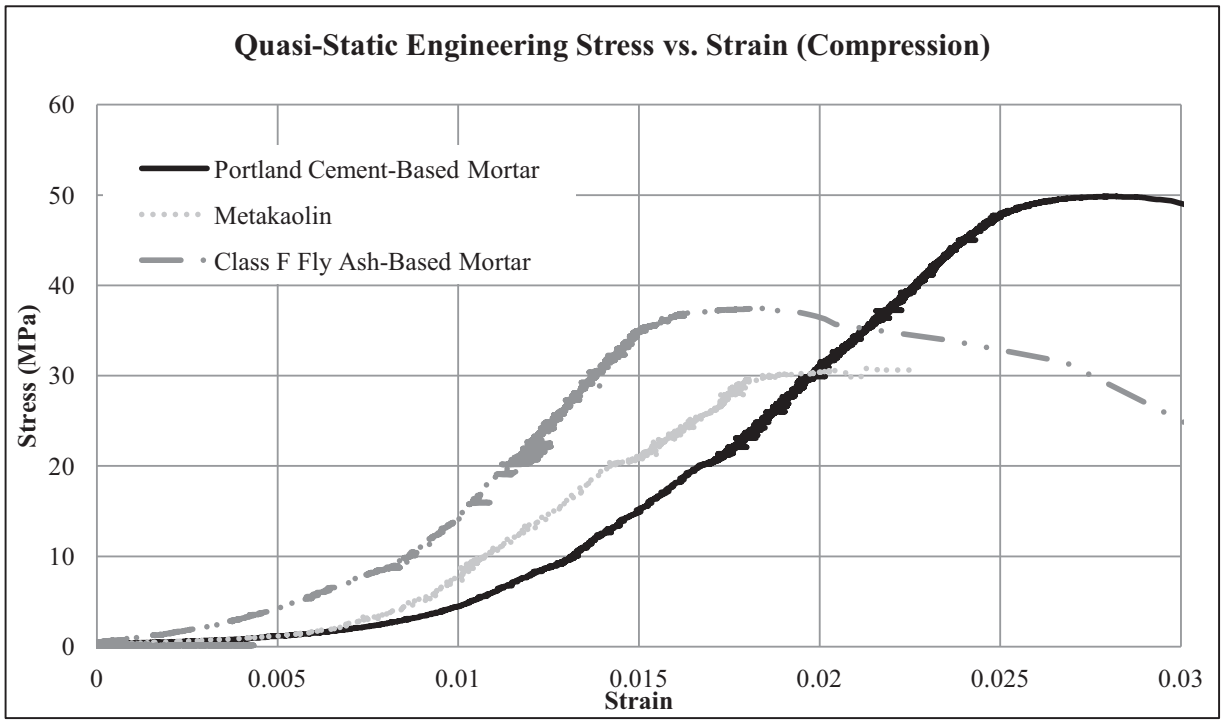

Figure 3.27 Quasi-Static Stress versus Strain for the Cementitious Materials Characterized

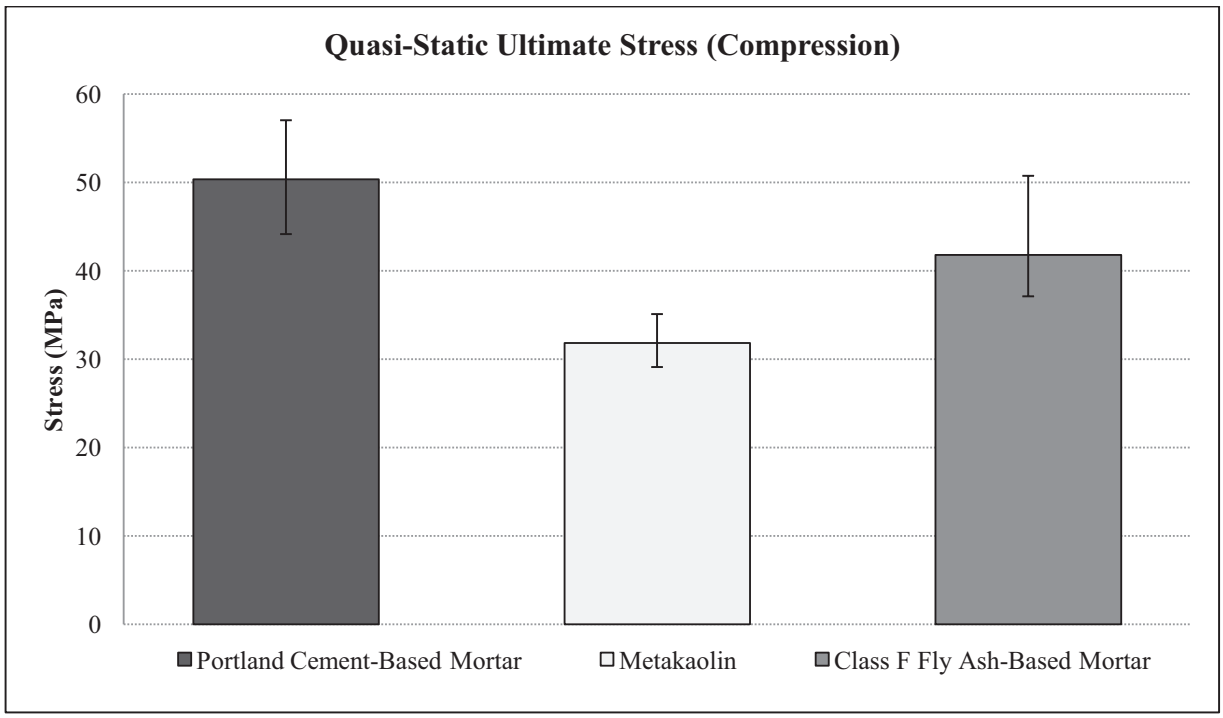

Figure 3.28 Quasi-Static Ultimate (Compression) Stress Results

III.VII Low-Velocity Impact

The Dynatup impulse data acquisition software provided instantaneous impact point displacement and applied load data. The load versus deflection data were plotted up to failure point for each tested sample. Cumulative energy absorption data were generated using approximate integration method (trapezoidal rule) [37].

$$E = \int_{x_{i-1}}^{x_{i+1}} P(x)dx \approx \frac{\Delta x}{2}[P(x_{i-1}) + 2P(x) + P(x_{i+1})] \quad 4.1$$

Where, P = instantaneous applied load and $\Delta x =$ increment of material deformation. Load vs. deflection plots show two distinct phases of failure propagation. The first phase is damage initiation which is the phase up until the peak load. The second phase which corresponds to the rapid reduction in load is called puncture propagation [39, 40]. These phases can be observed in figure 3.29. The total energy absorption was calculated as the sum of the energy absorbed for both damage initiation and puncture propagation phases up to complete failure of specimen. A typical energy absorption graph is shown in figure 3.30. The Portland cement-based mortar and fly ash-based mortar system both exhibited similar slopes of damage initiation; however, the fly ash-based mortar exhibited a decrease in energy absorption to damage initiation. The metakaolin based mortar system showed nearly a 50% decrease in absorbed energy to damage initiation. The Portland cement-based mortar exhibits a steep drop in energy required for puncture propagation, however, puncture propagation proceeds for a longer deflection than that of fly ash-based mortar. The metakaolin exhibited nearly a 50% decrease in energy required for damage initiation. This could be largely due to the brittle nature of metakaolin, the addition of sand in the other mortar systems, or a combination of both.

Under low velocity impact punch shear condition Portland cement-based mortar had the highest peak load, and class F fly ash-based mortar had the highest crack propagation energy.

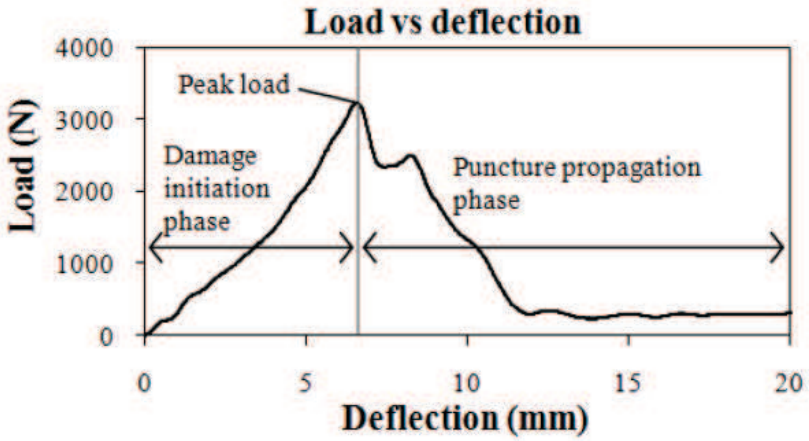

Figure 3.29 Low-Velocity Impact Load Versus Deflection Phases [28]

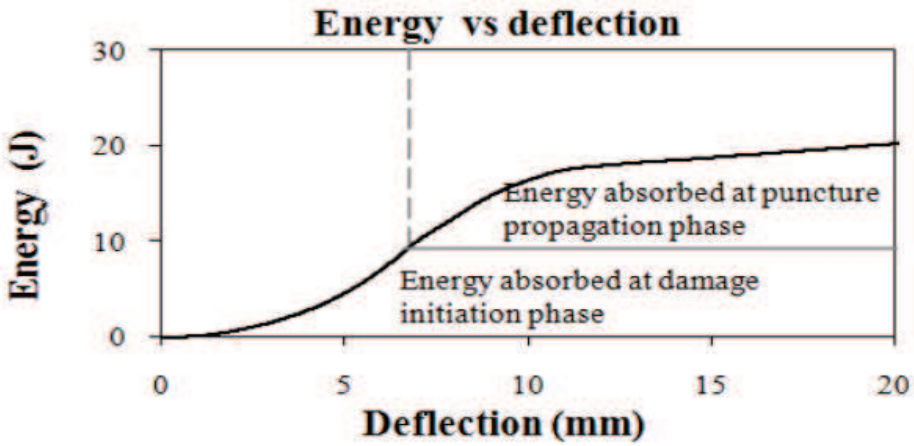

Figure 3.30 Energy Absorption Phases Under Low-Velocity Impact [28]

Figure 3.31 shows the experimental load versus deflection curve for typical response of the cementitious materials.

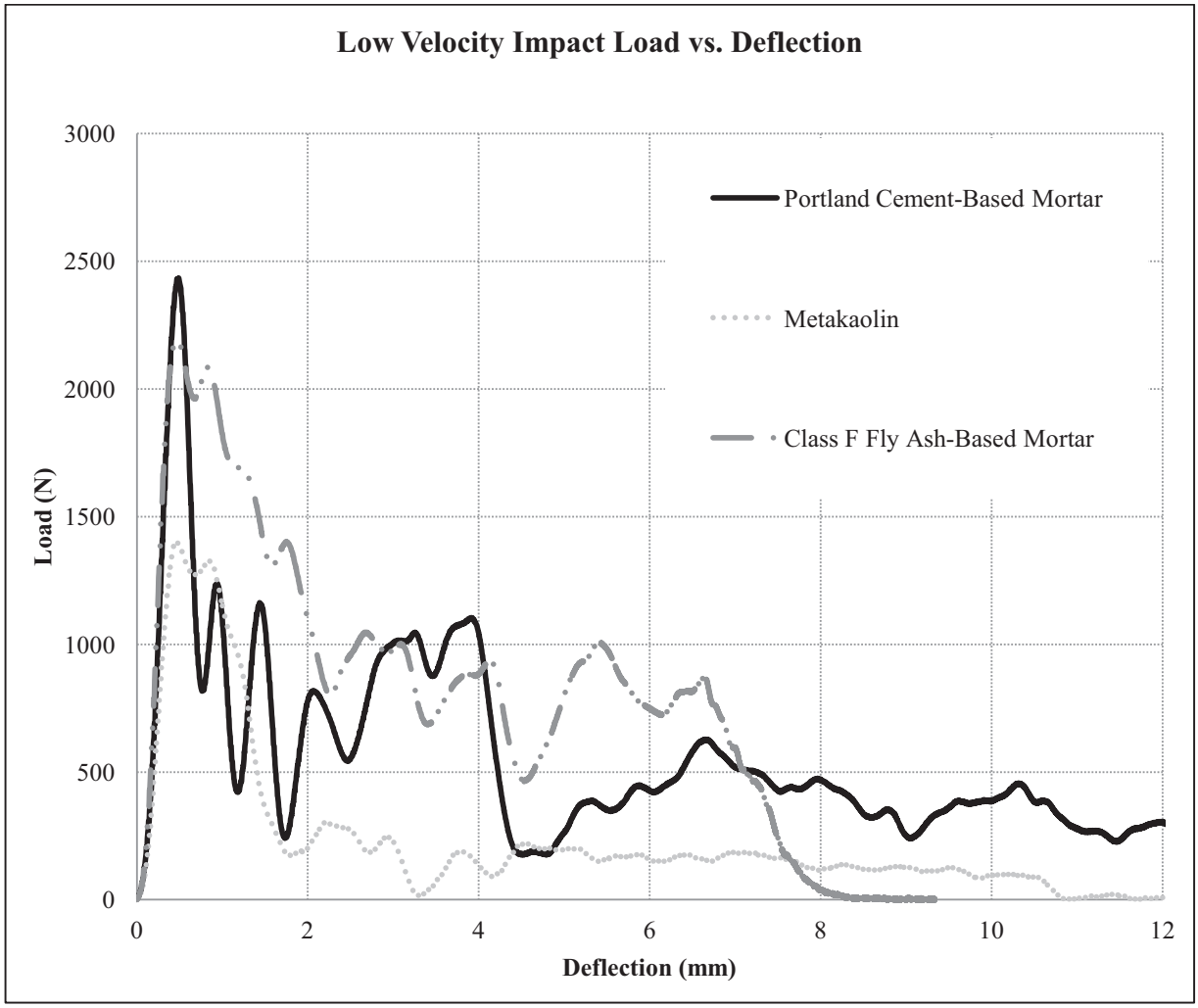

Figure 3.31 Load versus Displacement Under Low Velocity Impact

Figure 3.32 shows the total energy absorption of the cement mortars. The metakaolin required significantly lower amounts of energy for complete failure to occur. The difference in the energy required for complete failure of the Portland cement-based mortar and fly ash based mortar is approximately equivalent. The reason for these two observations could again be due to the presence of aggregates in the Portland cement-based mortar and fly ash-based mortar.

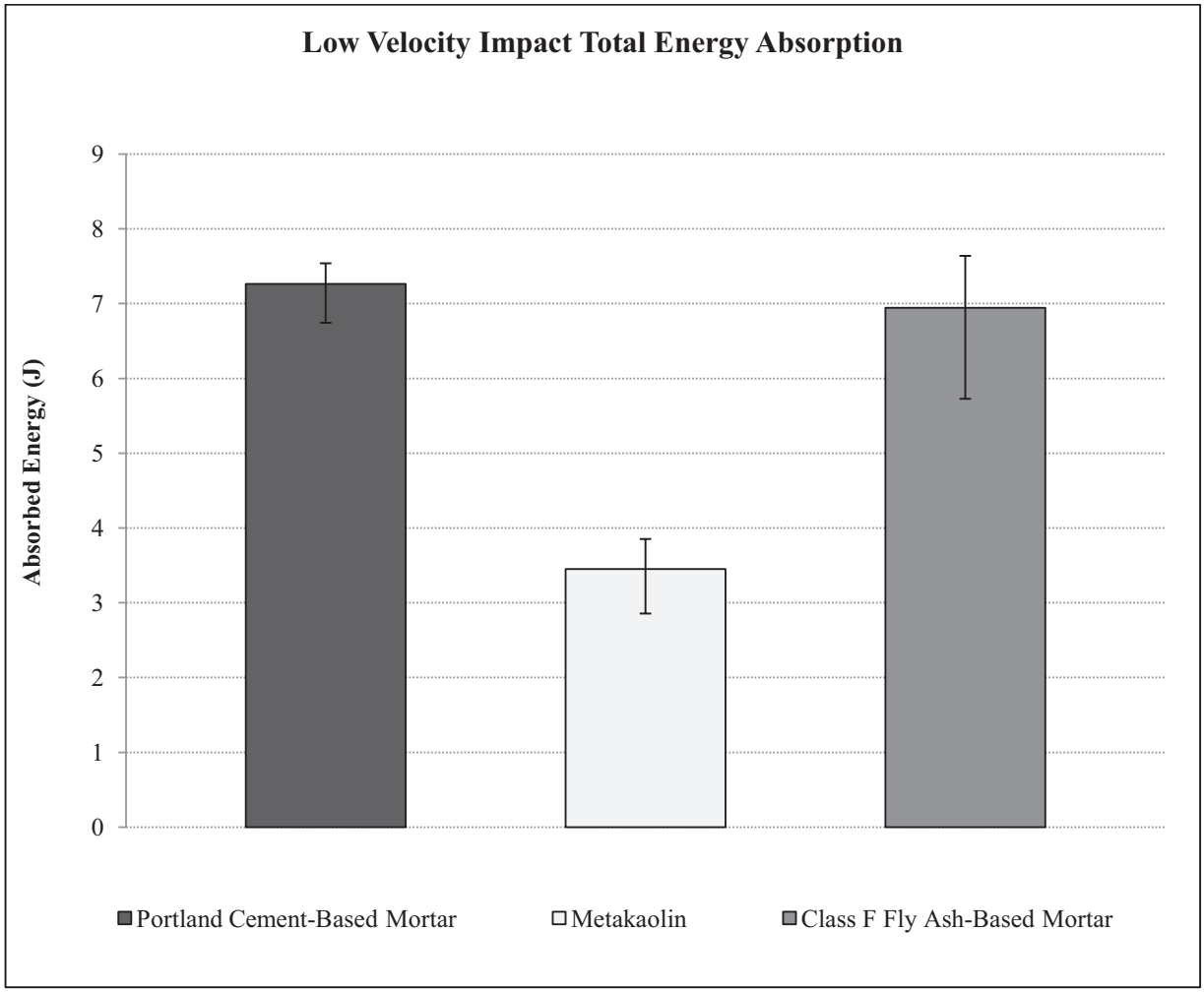

Figure 3.32 Total Energy Absorption Under Low Velocity Impact

III.VIII Split Hopkinson Pressure Bar (SHPB) Compression

The SHPB Compression analysis shows that the highest ultimate stress was for class F fly ash-based mortar, this difference in comparison to the highest ultimate stress for quasi-static and low velocity impact testing suggests the possibility of a different type of failure mechanism. The smallest critical strain (strain to failure) value for compression SHPB testing was class F fly ash-based mortar. The strain in the sample, stress in the sample, strain rate, and energy absorption capacity were calculated by equations 4.2 – 4.5.

$$\varepsilon_s(t) = \frac{C_o}{L_s}\int_0^t [\varepsilon_i(t) - \varepsilon_r(t) - \varepsilon_t(t)]dt \quad 4.2$$

$$\sigma_s = E_b \frac{A_b}{A_s}\varepsilon_t(t) \quad 4.3$$

$$\dot{\varepsilon} = \frac{-2C_o}{L_s}\varepsilon_r \quad 4.4$$

$$E = \int_0^{\varepsilon_s} \sigma \cdot d\varepsilon_s \quad 4.5$$

Where

C_o - wave speed

L_s – Sample Length

ε_i – incident strain

ε_r – reflected strain

ε_t – transmitted strain

E_b - modulus of elasticity of the incident bar

A_b – cross sectional area of the incident bar

A_s – cross sectional area of sample

E – Energy Absorption Capacity

Figure 3.33 shows the stress versus strain data obtained during SHPB testing. Figure 3.34 shows the ultimate strength during SHPB testing and scatter bands for the 3 samples tested. Figure 3.35 shows the energy absorption capacity of the 3 cementitious materials.

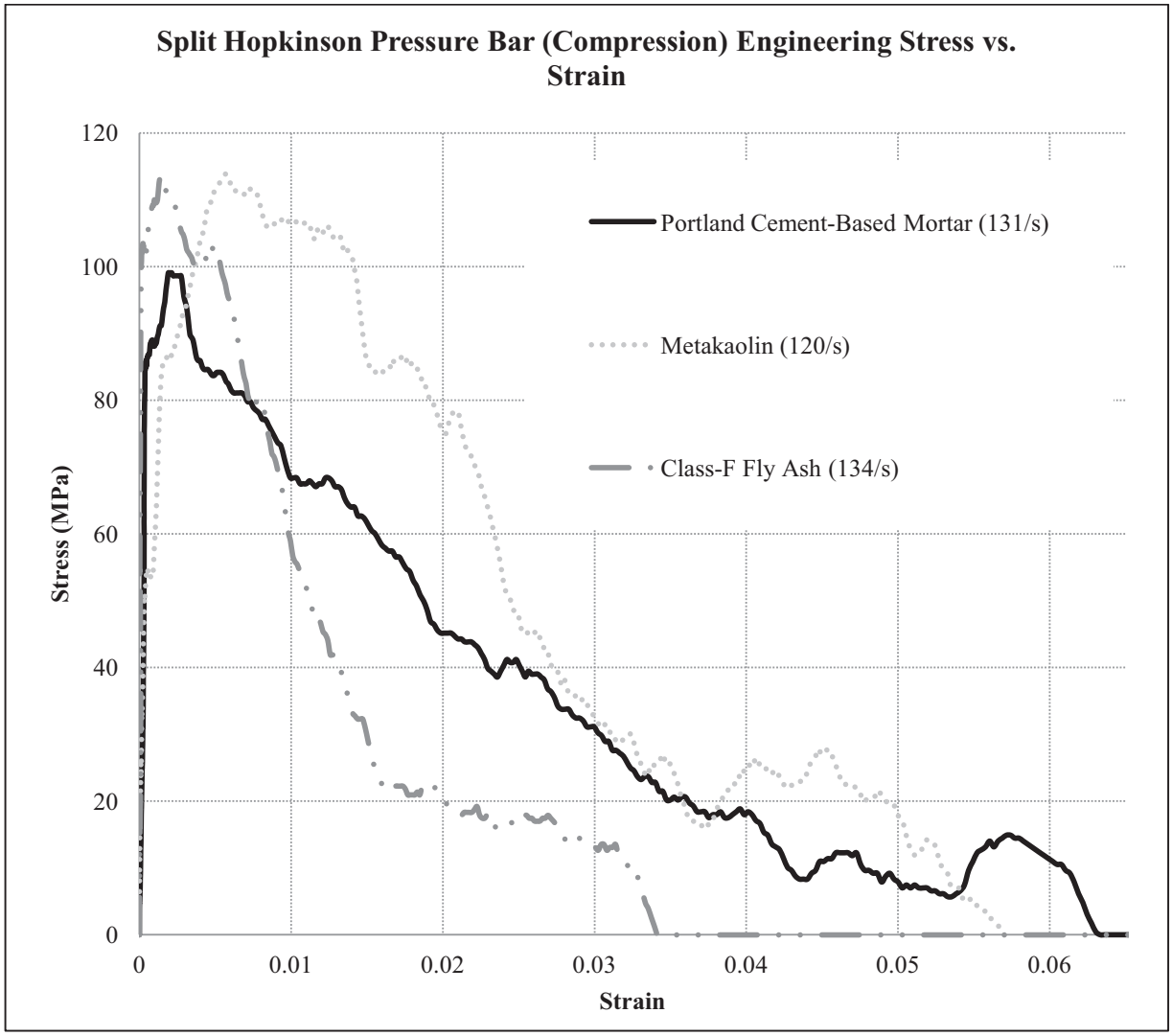

Figure 3.33 Split Hopkinson Pressure Bar (Compression) Engineering Stress versus Strain

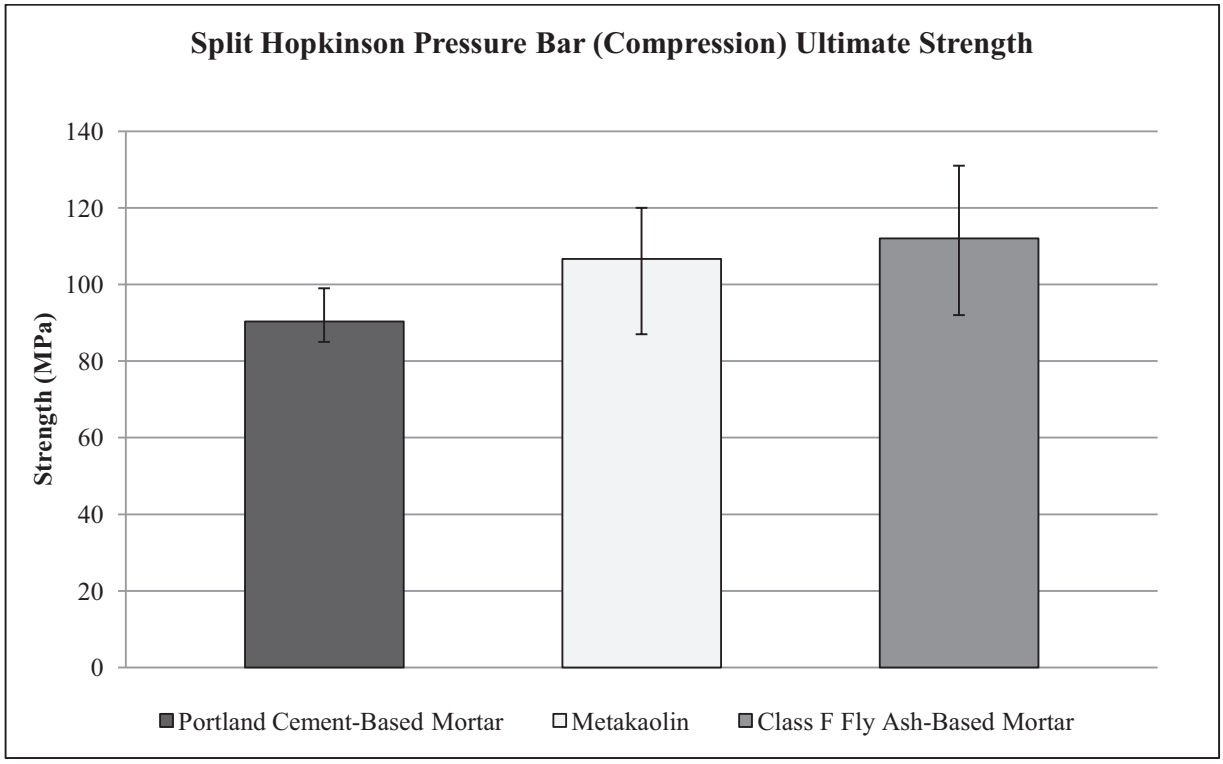

Figure 3.34 Split Hopkinson Pressure Bar (Compression) Ultimate Strength

The total energy absorption capacity (integral of stress versus strain curve) shows that metakaolin had the highest energy absorption capacity under compression SHPB testing. This increase in energy absorption could be due to the amount of energy necessary for pulverizing the metakaolin, as opposed to the incomplete crushing of very hard aggregates or launching of aggregates away from the loading location.

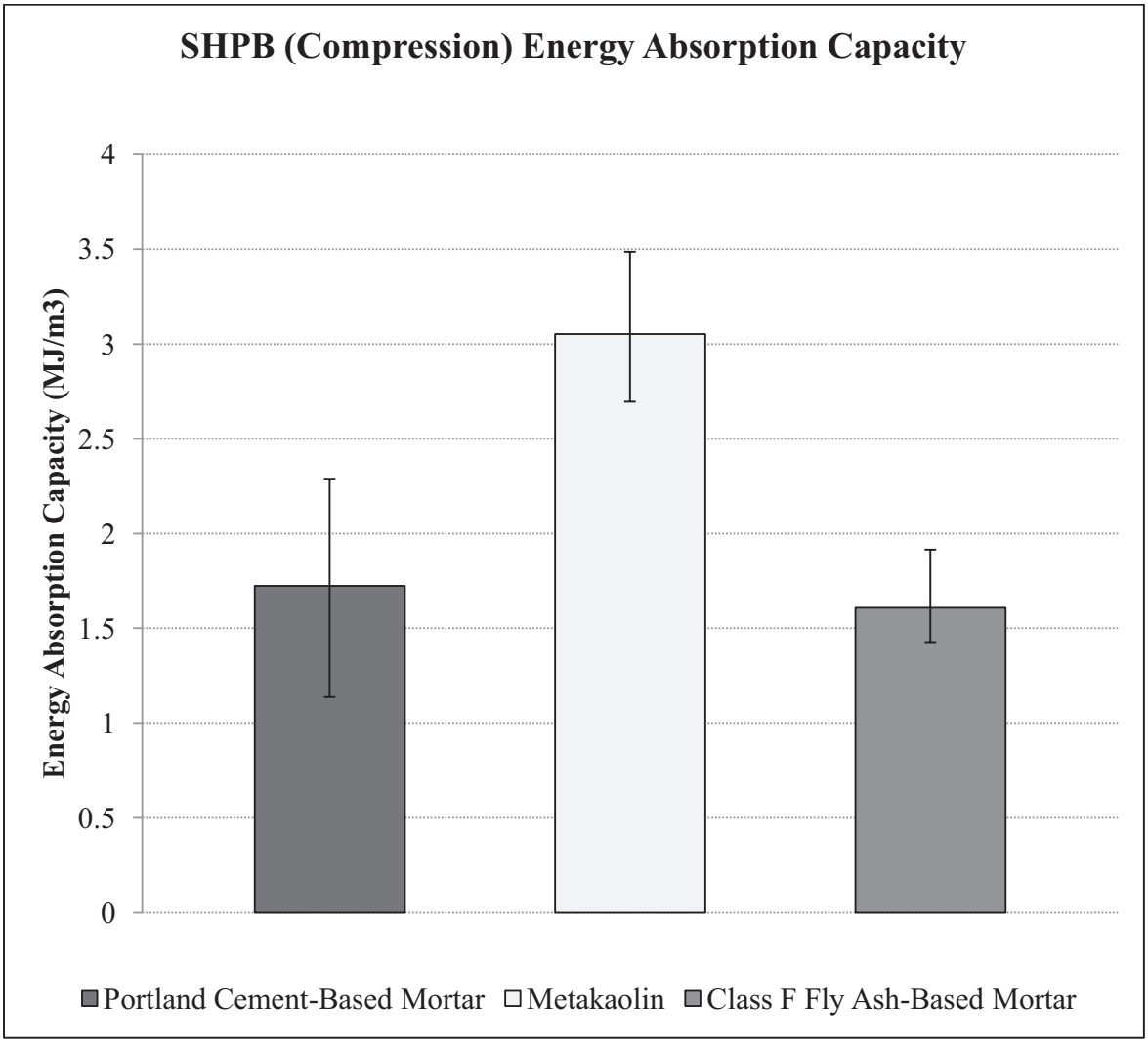

Figure 3.35 Split Hopkinson Pressure Bar (Compression) Energy Absorption Capacity

III.VIV Quasi-Static and SHPB Comparison

A comparison between the quasi-static and SHPB results show that the ultimate strength of each material increased under dynamic loading condition when compared to quasi-static. The results show that the strain to compressive failure is significantly lower under dynamic loading and the ultimate stress is higher under SHPB dynamic loading. Figure 3.36 shows the stress

versus strain comparison. Figure 3.37 shows the difference in ultimate strength for quasi-static loading and dynamic SHPB loading scenarios.

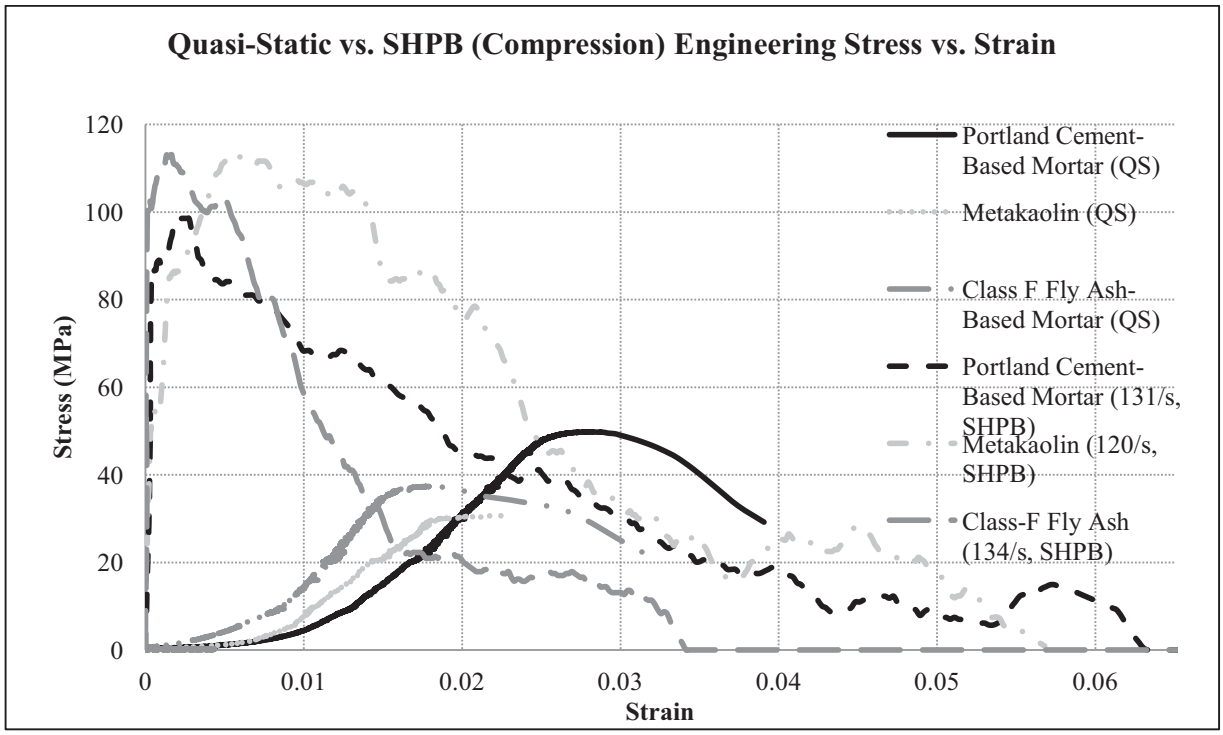

Figure 3.36 Quasi-Static vs. SHPB (Compression) Engineering Stress vs. Strain

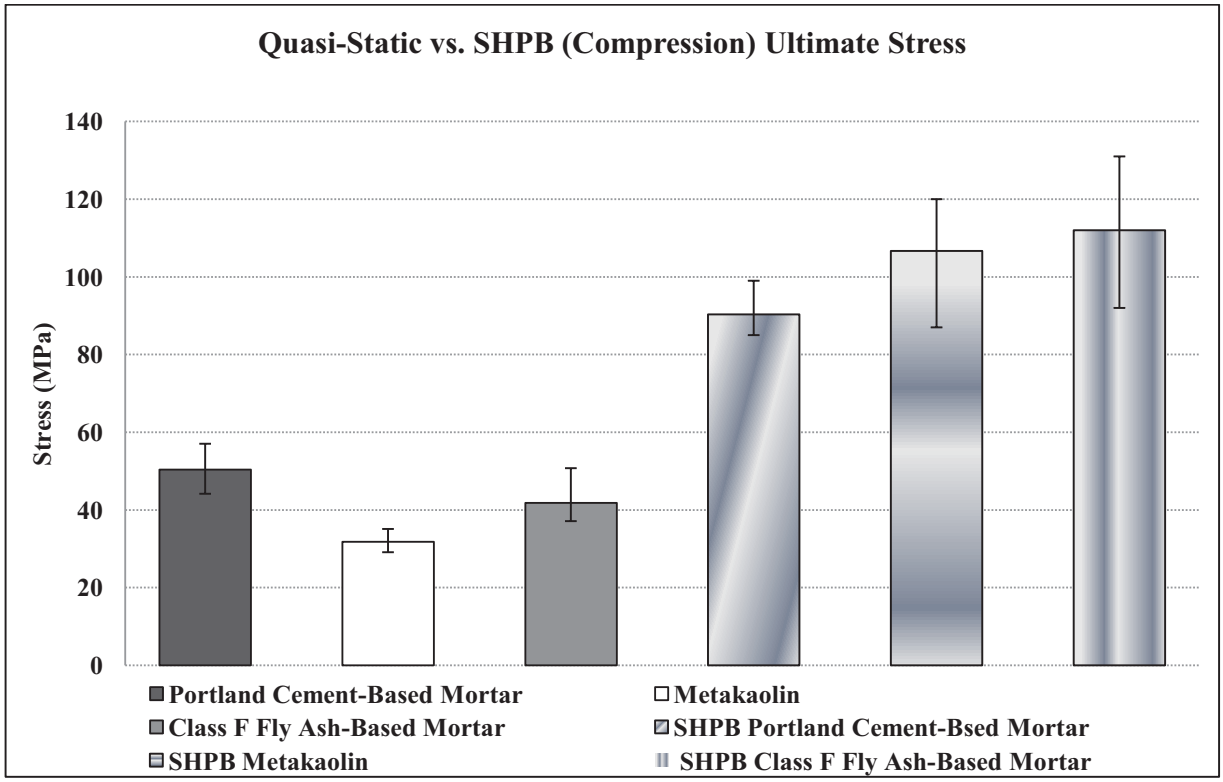

Figure 3.37 Quasi-Static versus Split Hopkinson Pressure Bar (Compression) Ultimate Strength

Using the volume measurements made during testing the energy absorption for each sample was calculated. Figure 3.38 shows the energy absorption comparison between the low velocity impact and SHPB results.

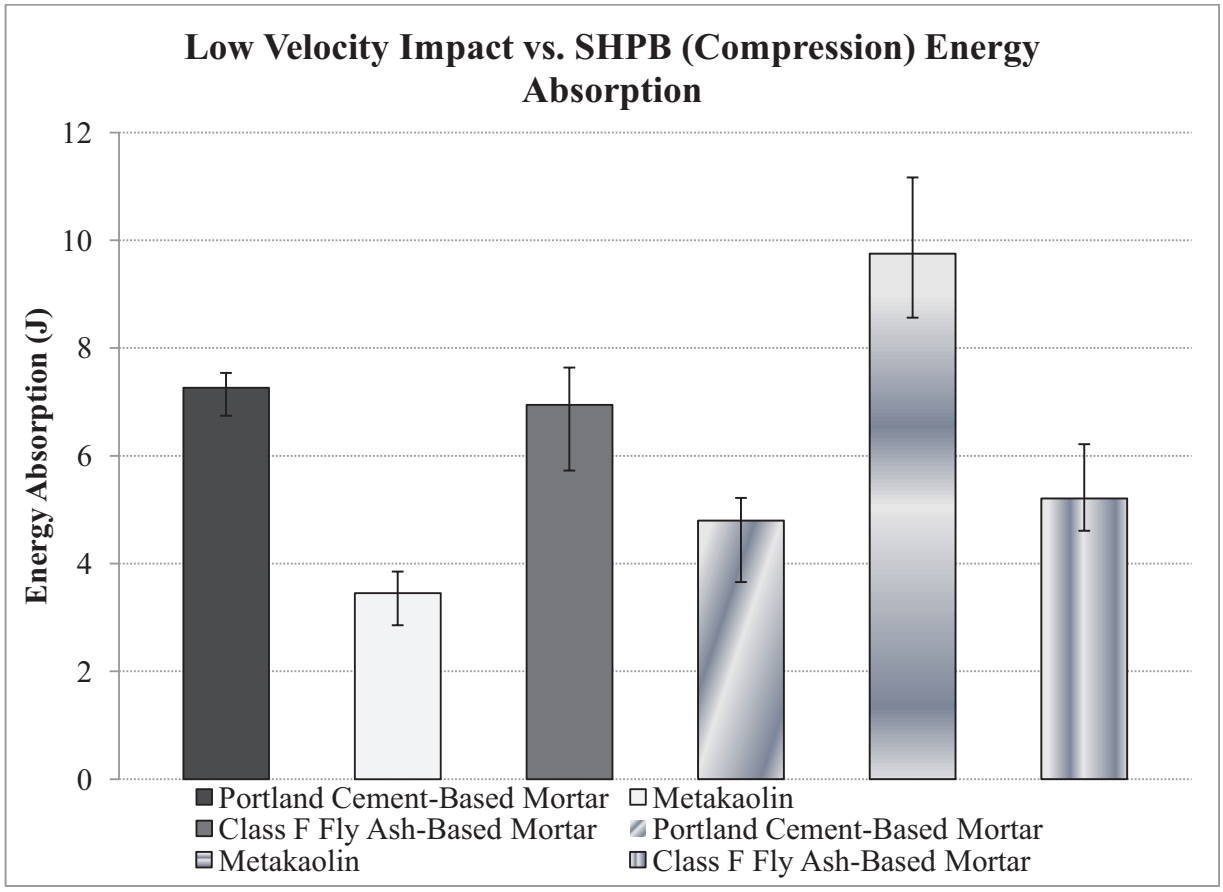

Figure 3.38 Low Velocity Impact versus Split Hopkinson Pressure Bar Energy Absorption

The Portland cement-based mortar and the class f fly ash based mortar had a decrease in energy absorption while the Metakaolin had a large increase in energy absorption.

III.VV LOEG

Due to the highly brittle nature of the cementitious materials tested, the global indirect tensile strain measured is much higher than the expected value during quasi-static and dynamic testing. During data reduction of both quasi-static and dynamic data it as observed that the strain to failure was approximately 0.015 or 1.5 % strain. The theroretical value for the tensile strain is approximately 0.00015 or 0.015 %. This exaggerated strain to failure was originally thought to be because the LOEG measures global strain, versus strain at the location near the crack.

However, using a high speed camera, images of the actual test were observed and showed that the local strain near the crack region and global strain when tensile failure occurs is close to zero. It was also observed that the strain of 0.015 or 1.5 % is well passed tensile failure. Figure 3.38 shows the high speed camera images at varying times during the SHPB indirect tensile test on Brazilian disc sample.

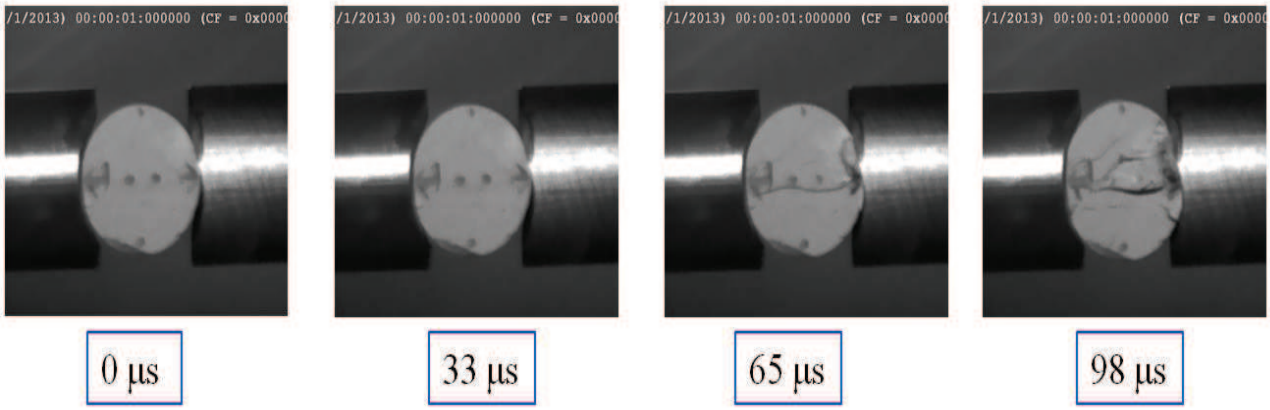

Figure 3.38 High Speed Camera SHPB Test at Varying Times on a Brazilian Disc Sample

At 33 µs the crack has started to propagate through the entire Brazilian disc sample, which is considered ultimate failure for tensile strength. At 65 µs the crack is clearly visible, and at 98 µs the sample has started to compressed. At the time interval of 33 µs and 65 µs the digital image correlation software shows zero percent strain. At 98 µs the strain is approximately 0.015 or 1.5 %. This clearly show that the strains that are measured during the LOEG are not due to the global strains, but are actually due to the two broken pieces of the sample being loaded in compression after tensile failure has occurred, and also debris blocking more of the LOEG laser sheet. It was also observed that the ultimate tensile failure strain was extremely small and was not able to be captured by the LOEG. After adjusting the data reduction parameters it was found that possible at best 5 data points could be captured, which could also be due to noise in the signal versus actual material response.

IV. CONCLUSION AND RECOMMENDATIONS

An investigation into the response of Portland cement-based mortar, metakaolin, and class F fly ash-based mortar at various strain rates has been conducted using an Instron 5980 Floor Model Universal Testing Systems Machine, a Dynatup low velocity impact testing machine, and a Split Hopkinson Pressure Bar system. Strain rate effects produced a dynamic increase of 1.5-2.2 for Portland cement-based mortars, 2.5-4.1 for metakaolin, and 1.8-3.5 for Class F fly ash-based mortar in ultimate compressive stress. Class F fly ash-based mortar had the highest total energy absorption under low velocity impact testing. Metakaolin had the highest energy absorption capacity under high strain rate compressive Split Hopkinson Pressure Bar testing. Low velocity impact test results show a 6% reduction in total energy to complete failure when comparing Portland cement-based mortar and a class F fly ash-based mortar, and a 45% reduction in total energy absorption when comparing Portland cement-based mortar to Metakaolin. Portland cement-based mortar had a decrease in energy absorption when comparing low velocity impact, Metakaolin had an increase in energy absorption, and class F fly ash-based mortar had a decrease in energy absorption.

Due to the highly brittle nature of the cementitious materials tested, the LOEG setup is not recommended for obtaining strain data for quasi-static and dynamic loading condition for brittle materials. Unless a consistent method of loading the sample until tensile failure occurs or more resolution in the signal is obtained, the LOEG will continue to give data past the point of tensile failure.

Future recommendation for this research is the use of more samples in the data collection process. Generally there is a lot of inconsistency in concrete mechanical properties even within the same batch. These inconsistencies are present in stress versus strain, ultimate strength, elastic modulus, elemental composition, and nearly every property of cementitious materials. Obtaining information from a large amount of samples would help to better understand the properties of the material and give the lower and upper ranges of use. This would allow better models of the material to be used in finite element analysis. It would also allow for less experimental testing in the future to be done because of improved models.

High speed digital image correlation would also be recommended with better resolution than achieved during this research. This would accurately obtain the tensile strain at failure and would also allow information about how damage is occurring and why different materials dissipate energy better than others.

REFERENCES

VI. REFERENCES

1. Ghorpade, Vaishali G., Rao, H. Sudarsana, "Chloride Ion Permiability Studies of Metakaolin Based High Performance Concrete," International Journal of Engineering Science and Technology (IJEST), Vol. 3, No. 2, 2011, pp 1617-1623
2. J. Temuujin, A. van Riessen, and K. MacKenzie, "Preparation and Characterization of Fly Ash Based Geopolymer Mortars," Constr Build Mater, 24 (2010) 1906-1910, 2010.
3. Patil, Sanjay N., Gupta, Anil K., Deshpande, Subhash S., "Metakoalin- Pozzolanic Material for Cement in High Strength Concrete," IOSR Journal for Mechanical and Civil Engineering, ISSN: 2278-1684, pp. 46-49, 2010.
4. Aleem, M., Arumairaj, P., Geopolymer concrete – A review, Int J Eng Sci & Emerging Tech, 1 (2012) 118-122.
5. FHWA, Geopolymer concrete, in: FHWA-HIF-10-014, Department of Transportation, Washington D.C., 2010
6. "Geopolymer". *Geopolymer*. 6 Nov, 2013. <http://en.wikipedia.org/wiki/Geopolymers>.
7. http://allysino.en.made-in-china.com/product/SbQJwVDHLjkv/China-High-Active-Metakaolin-MA-MK-.html
8. http://www.indiamart.com/renaissanceimpex/industrial-minerals.html
9. ASTM C618-12a, "Standard Specification for Coal Fly Ash and Raw or Calcined Natural Pozzolan for Use in Concrete," ASTM International, West Conshohocken, 2012.
10. "Fly Ash". *Fly Ash.* 6 Nov, 2013. <http://en.wikipedia.org/wiki/Fly_ash>
11. http://investor.fei.com/releasedetail.cfm?ReleaseID=267896

12. “Scanning electron microscope”. *Scanning electron microscope.* 6 Nov, 2013. <http://en.wikipedia.org/wiki/Scanning_electron_microscope>.
13. http://www.bruker.com/products/x-ray-diffraction-and-elemental-analysis/eds-wds-ebsd-sem-micro-xrf-and-sem-micro-ct/quantax-eds-for-sem/overview.html
14. “Energy-dispersive X-ray spectroscopy”. *Energy-dispersive X-ray spectroscopy*. 6 Nov, 2013. < http://en.wikipedia.org/wiki/Energy-dispersive_X-ray_spectroscopy>.
15. “X-Ray Fluorescence”. *X-Ray Fluoresence*. 6 Nov, 2013. <http://en.wikipedia.org/wiki/X-ray_fluorescence>.
16. http://www.panalytical.com/XPert-PRO-range.htm
17. “X-Ray Diffraction”. *X-Ray Diffraction*. 6 Nov, 2013. <http://en.wikipedia.org/wiki/X-ray_Diffraction>.
18. http://www.netzsch-thermal-analysis.com/en/products-solutions/simultaneous-thermogravimetry-differential-scanning-calorimetry/sta-449-f1-jupiter.html
19. “Thermogravimetric Analysis”. *Thermogravimetric* Analysis. 6 Nov, 2013. <http://en.wikipedia.org/wiki/Thermogravimetric_analysis>.
20. http://www.home.agilent.com/en/pd-1675520-pn-U9820A/agilent-nano-indenter-g200?&cc=US&lc=eng
21. http://www.hysitron.com/products/options/indenter-tips/
22. “Nanoindentation”. *Nanoindentation*. 6 Nov, 2013. <http://en.wikipedia.org/wiki/Nanoindentation>.
23. http://www.instron.us/wa/product/5980-floor-model-systems.aspx/
24. http://www.bose.com/controller?event=VIEW_STATIC_PAGE_EVENT&url=/endurate c/index.jsp

25. http://www.instron.us/wa/product/Drop-Weight-Impact-Testing-Systems.aspx
26. http://materials.iisc.ernet.in/~karthik/Facilities.html
27. “Split-Hopkinson Pressure Bar”. *Split-Hopkinson Pressure Bar*. 6 Nov, 2013. <http://en.wikipedia.org/wiki/Split-Hopkinson_pressure_bar>.
28. Pramanik, B. Dissertation Defense, “High-Strain Rate Tensile Characterization of Graphite Platelet Reinforced Vinyl Ester Based Nanocomposites Using Split-Hopkinson Pressure Bar”, Oct. 7, 2013, University of Mississippi
29. http://www.sigmaaldrich.com/catalog/product/sial/338443?lang=en&region=US
30. http://www.sigmaaldrich.com/catalog/product/sial/s5881?lang=en&region=US
31. Kuenzel, C., Vandeperre, L. J., Donatello, S., Boccaccini, A. R., and Chris Cheeseman., 2012, “Ambient Temperature Drying Shrinkage and Cracking in Metakaolin-Based Geopolymers,” The American Ceramic Society, 95[10] 3270-3277 (2012).
32. ASTM C778-13, “Standard Specification for Standard Sand” ASTM International, West Conshohocken, 2012.
33. Malone , P. G., Moser, R. D., Allison, P. G., Weiss Jr., C. A., Williams, B. A., Diaz, A., and Gore, R., 2011, “Improvement in the Geopolymer-to-Steel Bond Using a Reactive Vitreous Enamel Coating.
34. ASTM C109/109M-12, “Standard Test Method for Compressive Hydrualic Cement Mortars (Using 2-in. or [50-mm] Cube Specimens)[1],” ASTM International, West Conshohocken, 2012.
35. ASTM C469-02$^{\varepsilon 1}$, “Standard Test Method for Static Modulus of Elasticity and Poisson's Ratio of Concrete in Compression[1],” ASTM International, West Conshohocken, 2012.

36. ASTM Standard D3763, “Standard Test Method for High speed Puncture Properties of Plastic Using Load and Displacement Sensors,” ATSM International, West Conshohocken, 2006.
37. D. Hyde, “DPlot User Manual,” HydeSoft Computing LLC, Vicksburg, 2008.
38. Military Specification (MIL)-Handbook-17 (Vol. 1 – 5), Department of Defense Handbook, Polymers, Polymer Matrix Guidelines for Characterization of Structural Materials, (DOD, 17 June 2002)
39. Gama, B. A., Islam, S. M. W., Rahman, M., Gillespie Jr., J. W., Bogetti, T. A., Cheeseman, B. A., Yen, C. and Hoppel, C. P. R., “ Punch Shear Behavior of Thick-Section Composites Under Quasi-Static, Low Velocity, and Ballistic Impact Loading,” SAMPE Journal, Vol. 41, No. 4, 2005, pp. 6-13.
40. Broek, D., “Elementary Engineering Fracture Mechanics,” Martinus Nijhoff Publishers, Leiden, 1982. Doi: 10.1007/978-94-011-9055-8

VII. VITA

Born on July 8, 1985, the author of this M.S. Thesis, Damian Stoddard was raised by mother and father in Louisville, KY. The guidance and persistence of his parents led to the ambition to be a successful engineer. He was admitted to Prairie View A & M University in 2007 and was admitted to the mechanical engineering department. In May of 2010 he received his Bachelors of Science in Mechanical Engineering. He was then admitted to The University of Mississippi January 2011 to pursue his interest in blast and impact dynamics. Upon completion of this Thesis, he receives a Master of Science in Mechanical Engineering.